Electrodialysis of Potassium Chloride Solution using Iron Salt Embedded Zeolite Clay Composite Membrane

A Thesis Submitted

in partial fulfillment of the requirements for the degree of

Master of Technology

by

Satyam Agarwal

to the

DEPARTMENT OF CHEMICAL ENGINEERING
INDIAN INSTITUTE OF TECHNOLOGY, KANPUR

June, 2005

CERTIFICATE

It is certified that the work contained in the thesis entitled "**Electrodialysis of Potassium Chloride Solution using Iron Salt Embedded Zeolite Clay Composite Membrane**" has been carried out by **Satyam Agarwal** under my supervision and that it has not been submitted elsewhere for a degree.

Dr. Anil Kumar
Professor,
Department of Chemical Engineering
Indian Institute of Technology
Kanpur-208016.

ACKNOWLEDGEMENTS

Past two years that I spent working here for the M. Tech thesis, have been a great learning experience and thoroughly enjoyable. It would not have been so without the help of the people, I came in contact during this period. This is an opportune moment to thank them all.

First and the foremost, I would like to express my sincere thanks to my guide **Prof. Anil Kumar** for his inspiring guidance, friendly affection, unending encouragements and valuable suggestions. His vast experience and deep knowledge helped and influenced immensely every aspect of this work; yet he allowed great flexibility and freedom. His positive approach and methodological approach continues to enlighten my path.

I would like to thank all the faculty members of Chemical Engineering Department, IIT Kanpur who helped me a lot during my course work and for their useful suggestions. My special thanks to my senior lab mates Mr. G. Pugazhenthi, Manoj Kumar and Ajith Kumar with whom I worked during the initial part of my thesis, for their help and valuable suggestions. Above all, they have been good friends and companions.

I thank Ethaya, Subbu and Sonny ji for their availability for all type of discussions whenever required. They gave me a good company while working in late hours. My lab mates Jayasimha, Sunder Lal ji, Ram Pravesh, Jhansi ji and Anisia ji, need a word of appreciation for their help and for maintaining a good working atmosphere. I am also thankful, to Vishwakarmaji, Sharmaji and Chhotu for their constant help; to all my class mates, who made my stay so comfortable at IITK. My special thanks to my friends Nitesh, Warrier, Gajendra, Rajeev and Akhilesh for the unforgettable moments, which I had with them during my stay at IIT Kanpur. I express my hearty gratitude to my dear friend Sachin for sharing all my sorrows and pleasures.

Finally, I express my profound gratitude and affection to my parents and brother, for their encouragement, understanding, patience and support.

June, 2005 Satyam Agarwal

ABSTRACT

Iron salt embedded electrodialysis zeolite clay composite membrane has been prepared by in-situ hydrothermal crystallization of Analcime C zeolite over the mesoporous clay support followed by deposition of $FeCl_2$ inside the pores. The membrane has been used for the electrodialysis of potassium chloride solution and the results reported in terms of current efficiency, voltage drop and energy requirements. In addition, the effect of the current density, flow rate, salt and alkali concentration, and temperature on the performance of membrane is measured and reported in this work. A comparison of these results has also been done with that of sodium chloride solution. The current efficiency of our membrane is found to decrease slightly for higher current densities and higher alkali concentrations, increase at higher temperatures and higher salt concentrations and is little affected by flow rate. It has also been found that for the operating variables (temperature and salt concentration of anolyte chamber) which on increasing, increase the current efficiency, KCl solution gives better results than NaCl solution while for the operating variables (current density and concentration of catholyte chamber) which on increasing, decrease the current efficiency, NaCl solution gives better results than KCl solution. Our membrane gives a current efficiency of 90% at room temperature (30 ^{0}C, 0.1489 kWh/mol KOH, 127.3 A/m^2 and 2.0 N KCl solution) which increases with increase in temperature.

Contents

List of Tables

List of Figures

Chapter 1

INTRODUCTION

1.1 Electrodialysis

Electrodialysis is an electromembrane process in which ions are transported through ion permeable membranes. If two solutions are placed across the membrane, it would preferentially transport a given ion from one solution to another under the influence of a voltage between two end electrodes [1]. Therefore, electrodialysis can be used to separate a given ion selectively having positive or negative charge and reject ions of the opposite charge. Ion exchange membranes have well defined charge and acts as barriers between solutions in different compartments. For example, cation exchange membranes (negatively charged membranes) are permeable to cations while they are impermeable to anions.

Traditionally, electrodialysis was first developed for the desalination of saline solutions, particularly brackish water. Now in many areas of the world (particularly in deserts) it is the main process for the production of potable water. Other applications, such as the treatment of the industrial effluents, the production of boiler feed water, demineralization of whey and deacidification of fruit juices are gaining increasing importance with large scale industrial-installations. Some of the applications of electrodialysis are listed in Table 1.1. It has also been applied in lead (Pb^{2+}) separation from wastewater (using CR67, MK111, AR204SXR412 by Arak Petrochemicals, Ionics, USA) [17], recovery of tobacco polyphenols [18], radioactive iodine waste treatment [19], glycerol recovery in diester plants [20] and separation of catechins from tea leaves [21].

1.2 Electrodialysis Cell

Electrodialysis using a single anion or cation exchange membrane is known as membrane electrodialysis (Schematic diagram shown in Figure 1.1). Sometimes this is also called as membrane electro-hydrolysis because the electrolysis of water generates hydrogen ions and oxygen gas at the anode and hydroxide ions and hydrogen gas at the cathode [22].

Figure 1.1(a) shows the membrane electrodialysis setup when cation exchange membrane (CEM) is used. The salt solution (sodium nitrate) is pumped in the anode chamber and caustic soda solution in the cathode chamber. The solutions in the cathode and the anode chambers are known as catholyte (chamber I) and anolyte (chamber II) solutions respectively. When an electrical potential is applied across the electrodes, the sodium ions migrate from the anolyte to the catholyte solution through the membrane. This results in the formation of sodium hydroxide and nitric acid in the cathode and the anode chambers respectively due to electrode reactions. The electrode reactions can be shown as follows:

At the anode: $$\frac{1}{2}H_2O \rightarrow H^+ + \frac{1}{4}O_{2(g)} + e^- \tag{1.1}$$

At the cathode: $$H_2O + e^- \rightarrow OH^- + \frac{1}{2}H_{2(g)} \tag{1.2}$$

where e^- denotes an electron. The above electrode reactions are the same for all types of electrodialysis cells.

Figure 1.1(b) shows the schematic diagram when anion exchange membrane (AEM) is used. Here sodium nitrate solution and nitric acid are taken as the catholyte and anolyte solutions. The passage of current in this case is due to passage of nitrate ions.

When an electric potential is applied across the electrodes, the nitrate ions passes from the catholyte to the anolyte solution resulting in the formation of sodium hydroxide in the cathode chamber and nitric acid in the anode chamber respectively [23]. Thus, in both cases sodium hydroxide is always formed at cathode side while nitric acid is formed at anode side. The only difference is that we take salt solution in the cathode chamber while using AEM, whereas the salt solution is taken in the anode chamber when we use CEM. So the choice of the ion exchange membrane depends on whether we require the acid or the base [23].

The ion exchange membranes used in electrodialysis are of two types. The first type is homogeneous membranes which are composed of cross-linked polymers having ion-exchange groups covalently bonded to the polymer matrix. The methods of making homogeneous ion-exchange membranes belong to the following three different categories [24]:

1. Polymerization or polycondensation of monomers, at least one of them must contain a moiety which can be made anionic or cationic, respectively.
2. Introduction of anionic or cationic moieties into a preformed solid film.
3. Introduction of anionic or cationic moieties into a polymer, such as polystyrene, followed by dissolving the polymer and casting it into a film.

Some examples of the homogeneous membranes are poly (vinyl alcohol)/formyl methyl peridinium (PVA-FP) anion exchange membranes (Figure 1.2 a) [25], sulfonated polyphosphazene ion-exchange membranes (Figure 1.2 b) [26] and poly(2,6-dimethyl-1,4-phenylene oxide) (PPO) membranes (Figure 1.2 c) [27]. The second one is heterogeneous membranes in which there is a neutral polymer matrix (such as polyethylene, phenolic

resins or polyvinyl chloride) filled with micron sized particles of ion exchangers. In these, reasonable ion transport is found to occur if ion exchangers are present in the range of 50-70% by weight [28]. Such concentrations of ion-exchange particles are, in fact, the maximum possible concentrations for electrodialysis applications. Any attempt to obtain higher conductivity by increasing the concentration of ion exchanger beyond this range results in a loss of membrane strength and in reduced shape stability. This is due to increased swelling upon exposure of the membranes to aqueous salt solutions.

The membranes used upto now are mostly organic polymer in nature. The major commercial membranes are Nafion (DuPont), Aciplex (Asahi chemicals) and Flemion (Asahi glass). These are very expensive and are denatured at high temperature (above 100 ^{0}C). Polymeric cation exchange membranes have been prepared mainly either by sulfonation or radiation grafting of polymers. Generally, the sulfonated membranes have been prepared by reacting the polymer with 1:1 mixture of concentrated sulfuric acid and chlorosulfonic acid at 50 ^{0}C. Polymers used for these types of membranes are polystyrene, polyphosphazene, PS-DVB, poly (arylene ether sulfone), etc. [29-31]. In radiation grafting, polymer has been modified by graft polymerization with different monomers using radiation processing such as, radiation grafting of styrene/divinylbenzene onto poly (tetrafluoroethylene-co-perfluorovinyl ether) [32], radiation grafting of polyvinyledenefluoride (PVDF) followed by sulfonation reaction [33], etc. The desirable features of organic polymer membranes include their low electrical resistance and mechanical flexibility. The associated disadvantages are problems of selectivity, fouling and degradation at high temperature, which reduce efficiency of separation and life [34, 35].

In contrast the alkali selective ceramic membranes can provide higher current efficiency, can operate at higher temperature and as a result, manufacturing of ceramic membrane has undergone rapid growth in recent years. The rapidly changing environmental regulations in the use of chemicals and reagents also make them very attractive. For this purpose alumina supports are being used nowadays [36-39] and generally these supports are prepared by the gel-casting process. The process flow sheet of its preparation is shown in Figure 1.3 [40] and in order to impart ion exchange properties, these supports are immersed in a zirconia sol and then heated. After that, it is modified by dipping it in the solution of H_2PtCl_6 or H_3PO_4 and then calcined at around 300^0C [41, 42]. Other ceramic polymer composite membranes for electrolysis have also been reported in literatures [34, 35, 43 & 44].

1.3 Zeolite Membranes

Zeolites are three-dimensional, microporous, crystalline solids with well-defined structures that contain aluminum, silicon and oxygen in their regular framework. The silicon and aluminum atoms are tetrahedrally coordinated with each other through shared oxygen atoms forming $[AlO_4]^-$ and $[SiO_4]$ with the cations and water molecules are located in the pores. As the Si/Al ratio increases the stability of the zeolite increases and the cation exchange capacity (CEC) decreases. Zeolites have been extensively used for catalyst applications and the majority of World's gasoline is produced by the fluidized catalytic cracking of petroleum using this [45]. Use of zeolite ceramic composite membranes started in early 90's for gas permeation [46, 47] and after that these have been

used regularly for different type of separation processes e.g. permeation of binary mixtures, separation of surfactant by ultrafiltration etc. [46, 48-50].

Zeolites ceramic composite membranes have a number of advantages such as high thermal stability, cation selectivity, high mechanical strength, resistance to organic solvents, stability in basic alkali media, straight molecular size pores and a sharp pore size distribution. However, a thin defect-free film of zeolite is difficult to prepare [51, 52]. Preparation of Zeolite membranes on α-Al_2O_3 support has been reported [49, 53] and incorporation of zeolite into the pores of ceramic membranes as a way to obtain a microporous membrane has also been reported in the literature [46, 50].

Zeolites are usually synthesized under hydrothermal conditions in alkaline media at temperatures between about 80 and 200 °C. There are two processes in which a zeolite composite membrane can be prepared. They are direct in-situ crystallization and seeding supported crystallization. In first method the zeolite layer is synthesized in one step by hydrothermal crystallization of reaction mixture consisting of a silica source, an alumina source, an alkali (usually NaOH) and a structure directing surfactant molecule. A gel layer is formed on the support by precipitation of the silica sol under certain concentration ranges at a given temperature. The crystallization starts at the interface of the liquid phase (surfactant source) and the gel phase (silica source). The crystal grows into the gel consuming it until it reaches the support and in this process giving a continuous zeolite layer [46, 49, 50 & 53]. In the second method, the synthesis is a two step process consisting of a nucleation step followed by a crystal growth step. In the former, submicron sized zeolite particles are grown and then attached to the support, a procedure called seeding of the support. The seeded support is then subjected to the hydrothermal

crystallization during which the seeded crystals grow to form a continuous zeolite layer [54-56]. In addition, zeolite membranes can also be prepared by vapor phase transport method as well as using metal alcoholates in organic medium [51].

1.4 Objectives of the present work

In membrane cell process, the main points which should be emphasized are the stability of membrane, current efficiency, energy requirement and membrane cost. The ceramic membranes used earlier (e.g. NASICON) are highly stable and show comparable energy requirement with polymeric membranes, but costly and not easy to prepare. Due to high cation exchange capacity and long stability of zeolite membrane, we have decided to make this membrane and use it for electrodialysis of the salt solution.

The objective of the present work is to prepare a zeolite clay composite membrane which is modified by depositing the iron salt to reduce the potential difference across the membrane. This membrane is used for electrodialysis of potassium chloride solution. The effect of operating variables such as current density, base and salt concentration and flow rate of the solutions on the performance of electrodialysis in terms of current efficiency is to be studied and to be compared with the results of sodium chloride solution. Scaling up of the reactor is to be done for the nitration of PS-DVB and PMMA-EGDM resins.

Table 1.1: Applications of electrodialysis and related processes

S. No.	*Application*	*Membranes Used*	*References*
1.	Brackish water desalination	Cation-exchange membranes (CMXSb) and anion-exchange membranes (ACS), Tokuyama, Japan	2,3
2.	Recovery of acids	Anion-exchange membranes (AM-203), China	4,5
3.	Separation of NaCl from urine	Cation-exchange membranes (Type CR64 LMP-447) and anion-exchange membranes (Type 204-SZRA-412), Ionics, Inc. (USA)	6-8
4.	Recovery of Cr (III) and Cr (VI) from aqueous solution	Neosepta cation-exchange (CMX) and Tokuyama Soda anion exchange membrane (AMX), Eurodia	9,10
5.	Separation of nickel and cobalt	Sulfonated cation-exchange polyvinyldifluoride membrane	11
6.	Desalination of coal-mine brine	Commercial CMV, AMV membranes, Asahi Glass	12
7.	Remediation of copper mine tailings	Cation-exchange membrane (CMI-7000) and anion-exchange membrane (AMI-7001), Membranes International Inc.	13
8.	Separation of brine in presence of calcium sulfate	CMV and AMV, Asahi Glass membranes	14,15
9.	Separation of copper ions	Commercial anion and cation exchange membranes, Asahi Glass, Japan	16

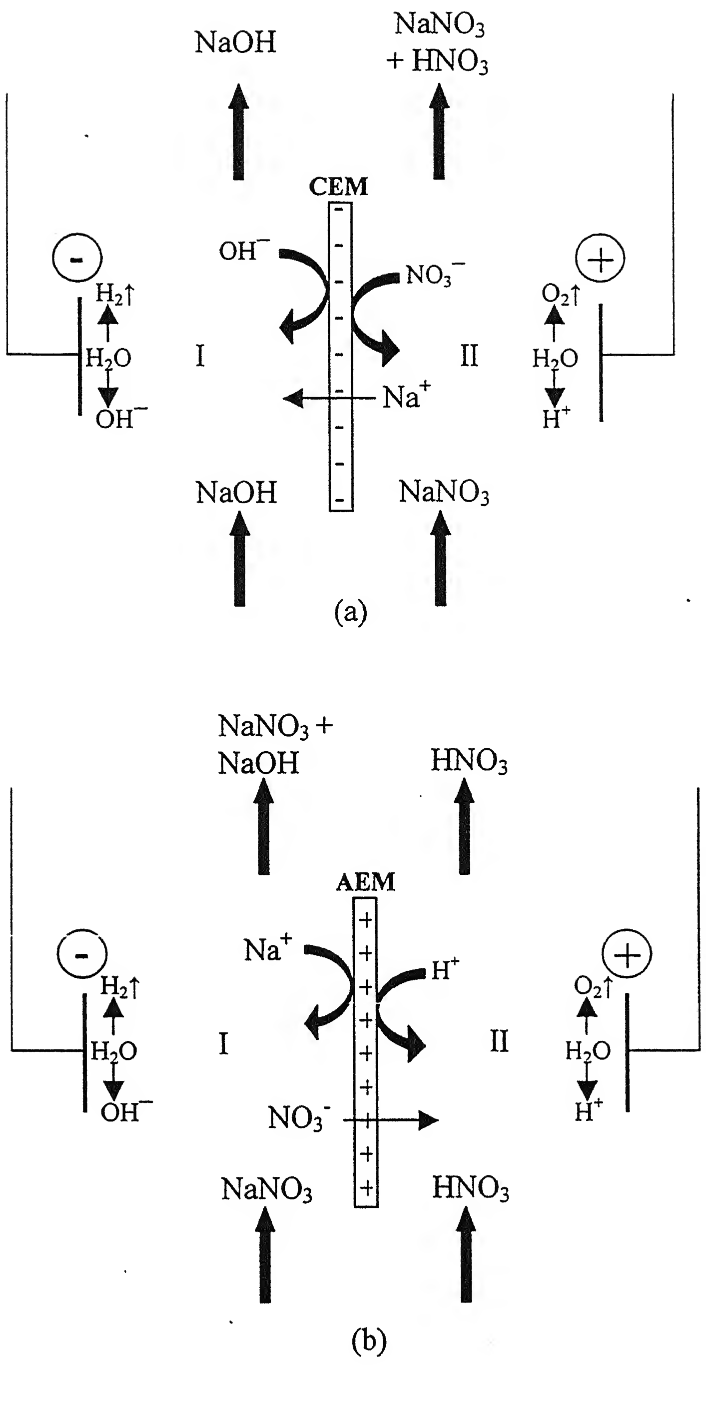

Figure 1.1: Production of Sodium Hydroxide and Nitric Acid from Sodium Nitrate with (a) Cation Exchange Membrane (CEM) and (b) Anion Exchange Membrane (AEM)

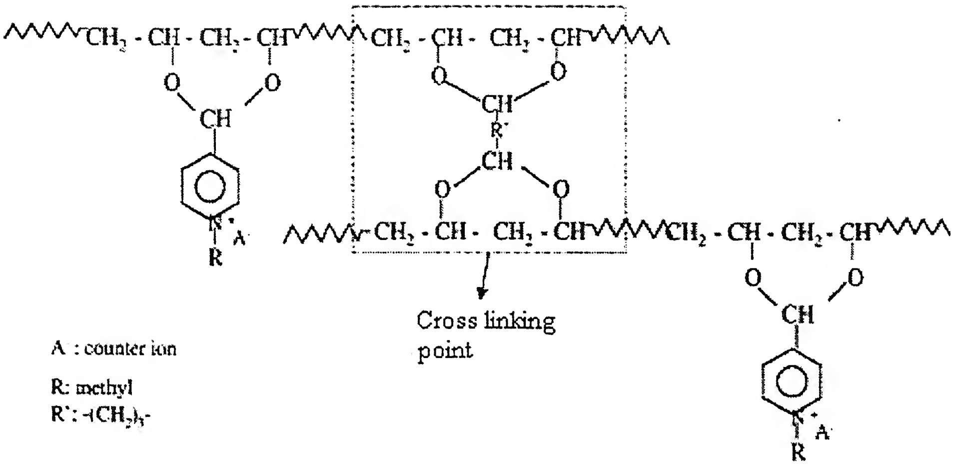

Cross-linked (PVA-FP)

(a)

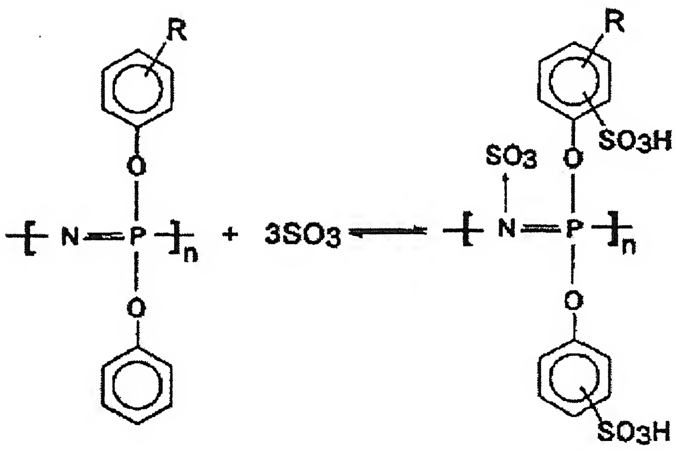

Sulfonated Polyphosphazene

(b)

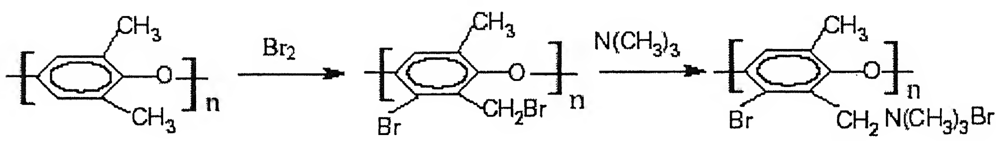

PPO

(c)

Figure 1.2: The chemical structures of (a) Cross-linked (PVA-FP) (b) Sulfonated Polyphosphazene (c) poly(2,6-dimethyl-1,4-phenylene oxide) (PPO)

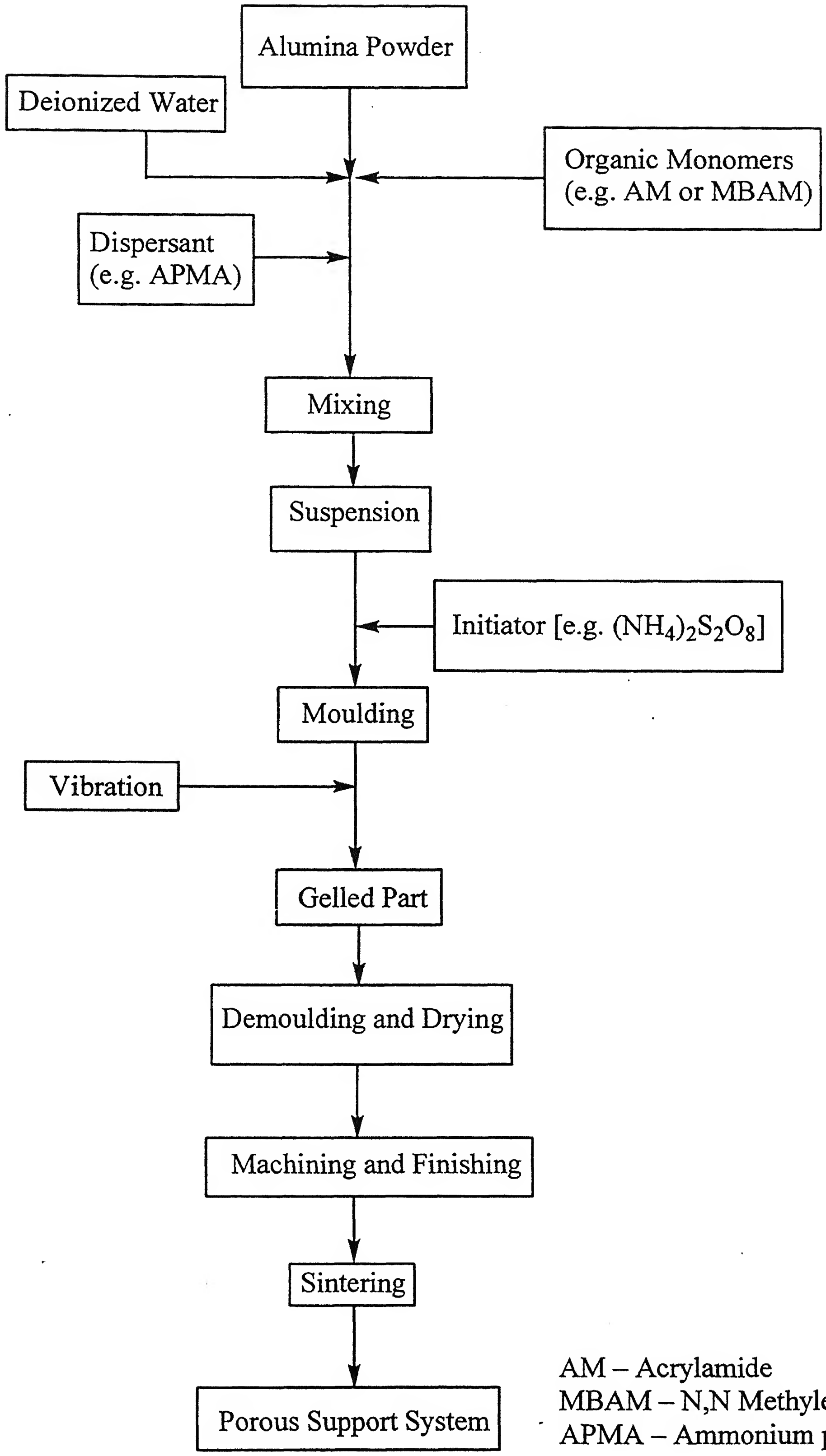

AM – Acrylamide
MBAM – N,N Methylene bis- acrylamide
APMA – Ammonium poly(methacrylate)

Figure 1.3: Flow sheet for the preparation of alumina support [40]

Chapter 2

EXPERIMENTAL SECTION

2.1 Materials Used

Clay raw materials such as kaolin, ball clay, feldspar, quartz, pyrophallite are obtained locally. Aluminium (metal) fine powder LR (99%), Calcium Carbonate special LR (98.5%), Ferrous Chloride anhydrous LR (96%), Oxalic acid purified LR (99.5%), Hydrochloric Acid LR (35-38%), Sodium Hydroxide (97%) and Potassium Hydroxide flakes LR (85%) have been purchased from s.d. fine–chem Ltd., Mumbai. The other chemicals used are Fumed Silica gel (AEROSIL 200, Sisco Research Laboratory, Bombay), Triethanolamine (97%, E. Merck (India) Limited, Mumbai) and Potassium Chloride (99.5%, Qualigens Fine Chemicals, Mumbai). All the above chemicals are used as received.

2.2 Preparation of the membrane

The ceramic zeolite membranes have been synthesized in following steps given below:

2.2.1 Preparation of clay discs

The macroporous clay supports have been prepared from the clay mixture with the composition given in Table 2.1 [50]. These clay powders were first thoroughly mixed and made into a paste by adding distilled water and is then cast over gypsum surface in the shape of a circular disc of size 76 mm diameter and 5 mm thickness. This was then

allowed to dry (for 24 h) after covering with a firebrick, to ensure the slow water removal. Further stages of drying are carried out at 100 ^{0}C for 12 hours, and then at 250 ^{0}C for 12 hours in an oven. This ensures the maximum removal of moisture and simultaneously avoids formation of cracks in the discs. After drying, the clay supports are sintered at 900^{0}C for 6-8 hours during which they become hard, rigid and macroporous in nature. During its drying at 100, 250 ^{0}C and sintering, the clay discs are placed vertically over the grooves of an insulation brick to ensure uniform drying/sintering. The sintered supports are slowly cooled down to room temperature and finally polished on a silicon carbide abrasive paper (No. C-220) to get the final smooth clay discs of thickness 2-3 mm and diameter 60 mm. Now, the clay discs are washed, kept in distilled water for a day to remove loose clay particles, and dried at 100 ^{0}C for 12 h.

2.2.2 Slipcasting of clay supports

Macroporous clay supports prepared as above are converted to mesoporous supports by coating them with a thin mesoporous film of kaolin solution (50 wt %) until its pores are filled up by the solution. It is then taken out and dried at 100 ^{0}C in an oven for 24 h. After that, it is sintered at 900 ^{0}C for 8 h during which the kaolin deposited inside the pores condensed into hard material.

2.2.3 Synthesis of iron salt embedded zeolite clay composite membrane

Zeolite (Analcime-C) film is grown hydrothermally over the mesoporous clay support following the procedure given in literature [57]. The composition of the reaction mixture has been taken as 4.5 Na_2O : Al_2O_3 : 4.5 SiO_2 : 380 H_2O : 6.1 TEA, where TEA is

Triethanolamine which serves as a structure-directing agent. About 200 ml of a reaction mixture of the composition given above is taken and stirred for an hour to form a gel-like solution (composition of the synthesis gel given in Table 2.2). A clay support is placed at the bottom of a steel Parr autoclave (1 liter volume), then the gel-solution is poured over it and subjected to hydrothermal crystallization at 200 ^{0}C. To study the effect of reaction time on zeolite formation, we run the reaction for 3, 6, 12, 24, 48 and 72 h. After the reaction, the discs are thoroughly washed with distilled water and dried at 100 ^{0}C in an oven for 24 h followed by calcination at 325 ^{0}C during which the organic surfactant (triethanolamine) is burnt leaving an open pore zeolite framework.

In order to deposit the iron salt ($FeCl_2$), the zeolite filled clay composite membrane is boiled in the $FeCl_2$ solution (having concentration of 20 g/lit) for 12 h at 60^{0}C [58]. During the boiling, $FeCl_2$ is trapped inside the pores. To avoid the leaching of $FeCl_2$, both sides of the membrane are coated with a tetraethyl orthosilicate (TEOS) solution, with a molar ratio of 1 TEOS : 2 H_2O : 0.04 HCl [59]. Then the coated membrane is maintained at 100 ^{0}C for 12 hours followed by drying at 200 ^{0}C for 8 h.

2.3 Characterization of the Membrane

The membrane has been characterized with the following techniques:

i. X-ray diffraction (XRD) of the zeolite powder

ii. Scanning electron microscopy (SEM) of the membrane

iii. Cation exchange capacity of deposited zeolite powder

iv. Pore size distribution of the membrane

v. I-V curve for the membrane

2.3.1 X-ray diffraction

XRD analysis was done using the zeolite powder collected from the bottom of autoclave. The XRD pattern was recorded in a Model Iso-Debye Flux 2002 X-ray powder diffractometer (Rich Seifert & Co., Germany). The Cu Kα radiation was used as X-ray source with accelerating voltage of 30 kV and tube current of 20 mA. The diffraction pattern was recorded using relative intensity as a function of 2θ at constant wavelength of 1.5406 A^0. Relation between wavelength of the incident X-radiation (λ), interatomic spacing (d) and angle of diffraction (θ) is given by Bragg's law:

$$n\lambda = 2d\sin\theta$$

2.3.2 Scanning Electron Microscopy (SEM)

The structural morphology of the zeolite layer was examined by a Joel 840 A scanning electron microscope. Membrane sample is first applied in liquid nitrogen and then coated with gold before carrying SEM analysis.

2.3.3 Determination of Cation Exchange Capacity

To determine the cation exchangeability of zeolite powder collected from the bottom of the autoclave [61], approximately 1 g of hydrated calcium chloride is dissolved in 1.1 litre of distilled water and pH is adjusted to 9-9.5 using buffer solution. 100 ml of this Ca^{++} solution is taken out for analysis of Ca^{++} content. Now, 1 g of oven dried zeolite is mixed and stirred with rest of Ca^{++} solution for 1 h at room temperature. After this the solution is filtrated and filtrate is collected to find the Ca^{++} content. From the difference between concentration of original solution and filtrate, the cation exchange capacity is calculated as milli-equivalent per gram of the dried zeolite.

The concentration of calcium ions in the solution is determined by titration with EDTA (Ethylene diamine tetra-acetic acid). The titration is carried out in presence of indicator, Eriocrome Black T (alcoholic solution of a blue dye) and buffer solution (mixture of NH_4Cl and ammonia water) to maintain a pH of about 10. End point changes from wine red color to blue [60]. The cation exchange capacity of zeolite is found by following relation [61]:

$$CEC = \frac{(A-B)}{C.D} X10 \qquad (2.1)$$

Above, A is volume (in ml) of 0.01M EDTA solution consumed for original Ca^{++} solution, B is volume (in ml) of 0.01M EDTA solution consumed for exchanged Ca^{++} solution, C is ml of sample taken for titration, D is mass of oven dried zeolite taken for exchange (in gram). The result of cation exchanging sodium zeolite with calcium ion is due to the formation of calcium zeolite. Mixing with 10% sodium chloride solution for one hour converts this Ca-zeolite into the Na-zeolite.

2.3.4 Pore size distribution

The bubble point technique is used to determine the pore size distribution of single cycle deposited zeolite clay composite membrane, six cycles deposited zeolite clay composite membrane and iron salt embedded membrane (after six cycles of deposition of zeolite). This technique is well suited for the asymmetric membranes and is based on the principle of the resistance offered to the displacement of a wetting liquid by a non-wetting liquid. The differential pressure (ΔP) required for the displacement is given by the Laplace equation [50, 62]:

$$\Delta P = \frac{2\sigma\cos\theta}{r} \tag{2.2}$$

where, σ is the interfacial tension between the two fluids and θ is the contact angle between the fluids and the solid (zeolite). The bubble point setup (as shown in Figure 2.1) used for this experiment consists of a stainless steel (SS 316) tubular cell with a flat circular SS 316 base plate which contains the membrane housing. The membrane is placed in a stainless steel casing and sealed with an epoxy resin. We used water as the wetting liquid and butanol as the non-wetting liquid. The membrane is then kept in distilled water to fill the pores with water (wetting liquid). After that, the wet membrane is placed in the membrane housing. The tubular section is filled with butanol and the whole cell is then pressurized with compressed air. The butanol flux is noted for different applied pressures.

2.3.5 Current-Voltage characteristics

The current-voltage curve was determined by using a test cell shown in Figure 2.2. This cell consists of two compartments arranged between Platinum anode and stainless steel cathode with membrane at the center. The voltage drop across the membrane is measured using two Ag/AgCl electrodes. The membrane is first equilibrated in salt solution of concentration 1 mol/lit for 24 hours and the two compartments are rinsed with the salt solution. Before the actual experiment, compartments were first filled with salt solution and circulated using peristaltic pumps for a couple of hours to reach an equilibrium state. The current voltage curve was obtained by applying a potential difference across the cell via a DC source and allowing the current to reach a steady state value [63, 64].

2.4 Experimental Set up for the Electrodialysis

The experimental setup (made up of Perspex) used for electrodialytic splitting using the membrane is shown in figure 2.3. It has two detachable compartments, each having 75 ml volume, with provision for fixing a membrane between the compartments. The inlets are connected to peristaltic pumps, which allow a continuous flow of the solutions. There are two electrodes on the farther ends of the two compartments. Cathode is made of Stainless steel and anode is made of Platinum with the exposed area of the membrane as 19.635 cm^2. The anolyte (KCl) and the catholyte (KOH) are circulated with a solution pumped from two 1 liter glass reservoirs using peristaltic pumps. Throughout the electrodialysis experiment, the solutions are stirred with magnetic stirrers and the power is supplied using constant DC source. A potential difference is applied across the electrodes and it is varied accordingly to maintain a constant current density through the membrane.

The performance of the membrane was studied under the different current densities (127.3, 254.6 and 509.2 A/m^2), circulating flow rates (33, 100 and 165 ml/min), anolyte salt concentrations (1.5, 2.0 and 3.0 N), catholite concentrations (0.1, 0.2 and 0.5 N), and temperatures (30, 50 and 70 ^0C). When the experiments were performed to determine the influence of one parameter, the other variables were kept constant at the conditions of 30 ^0C, 33 ml/min, 254.6 A/m^2, 0.2N KOH and 2.0N KCl. Samples of catholite are taken every 30 min and the concentrations of KOH measured volumetrically by titration with Oxalic acid using phenolphthalein as indicator. Each electrodialysis run typically proceeded for 150 min under the chosen operational conditions. We also compared all these results of KCl solution at different operating parameters with that of

NaCl solution. Electrodialysis of NaCl solution was done by Manoj [65]. For the determination of the energy consumed, the voltage is assumed to be approximately constant between two readings. The current efficiency (%) and the energy consumed (kWh/mol KOH produced) are determined by the following formulae:

$$\eta = \frac{\Delta C \cdot \mathrm{v}}{\left(I \cdot \Delta t / F\right)} X100 \tag{2.3}$$

$$E = \frac{V_{Avg} \cdot I \cdot t}{\Delta N \cdot 1000} \quad \text{kWh/mol of KOH produced} \tag{2.4}$$

where ΔC is the change in concentration of KOH (mol/lit) in time Δt seconds, v is the volume of catholyte solution in lit, I is the current in amperes, F is the Faradays' number, V_{Avg} is the average cell voltage for each electrodialysis run, and ΔN is the moles of KOH formed during the electrodialysis run for time t.

Table 2.1: Composition of clay minerals for making supports

Clay raw material	**Chemical Formula**	**Composition (wt. %)**
Kaolin	$Al_2(Si_2O_5)(OH)_4$	10.15
Ball clay	$3SiO_2.Al_2O_3$	12.90
Feldspar	$(Na, Ca)(AlSi_3O_8)$	4.08
Quartz	SiO_2	18.85
Calcium carbonate	$CaCO_3$	22.52
Pyrophyllite	$Al_2(Si_2O_5)_2(OH)_2$	11.50
Water	H_2O	20.00

Table 2.2: Composition of synthesis gel

Compound	**Chemical Formula**	**Weight (g)**
Aerosil 200 (fumed silica gel)	SiO_2	4.188
Aluminum metal powder	Al	0.881
Sodium hydroxide	NaOH	5.585
Triethanolamine	$N(CH_2CH_2OH)_3$	12.20
Distilled water	H_2O	200

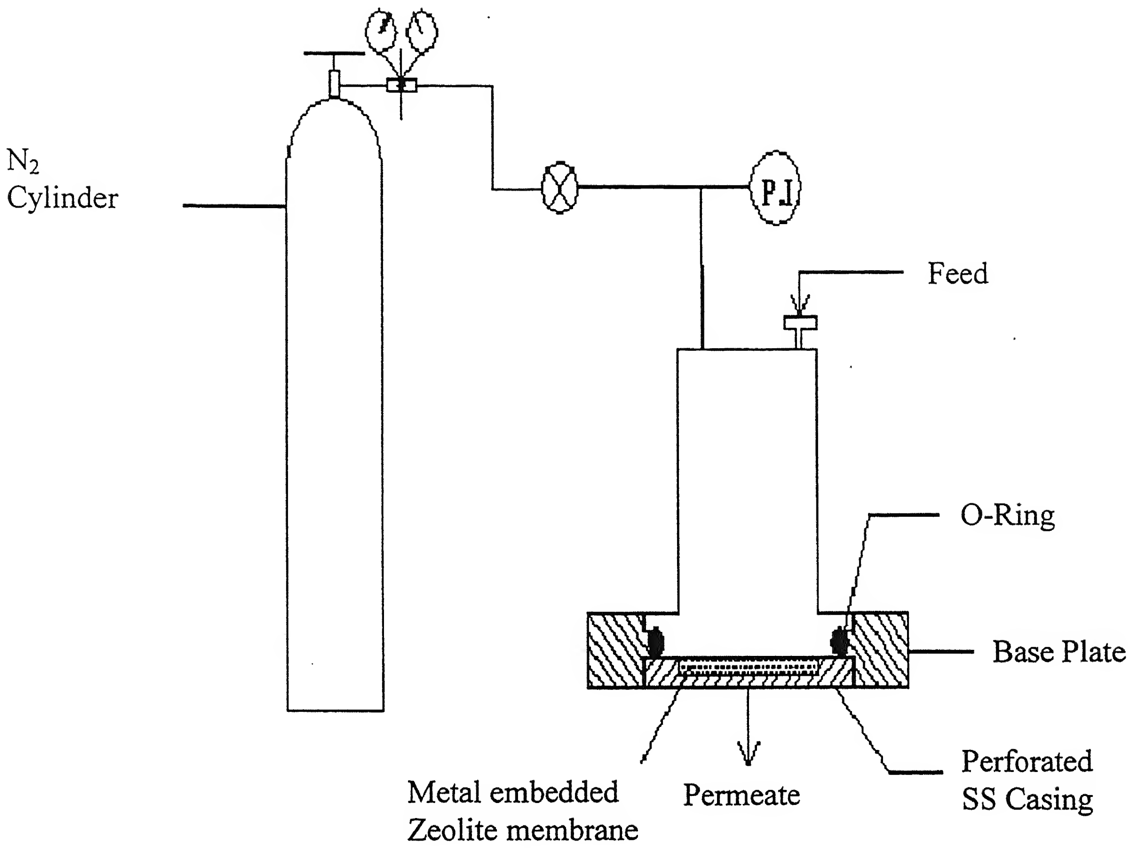

Figure 2.1: Experimental setup for the Bubble point technique

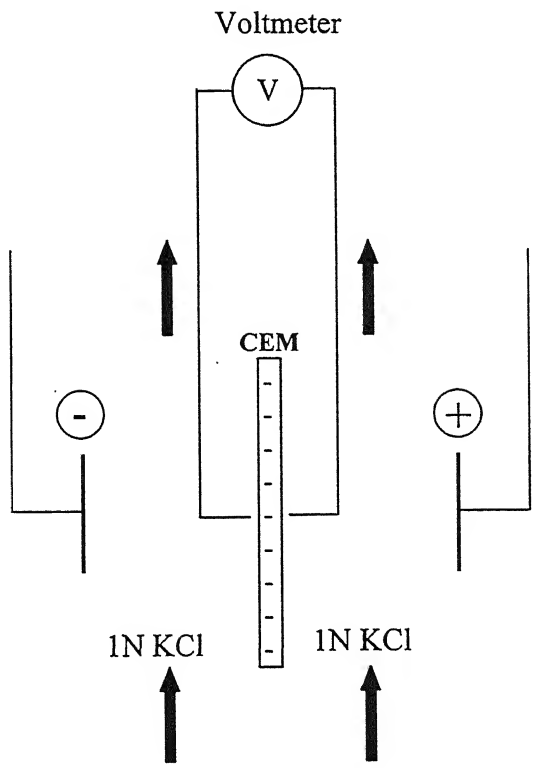

Figure 2.2: Experimental setup for current-voltage measurements

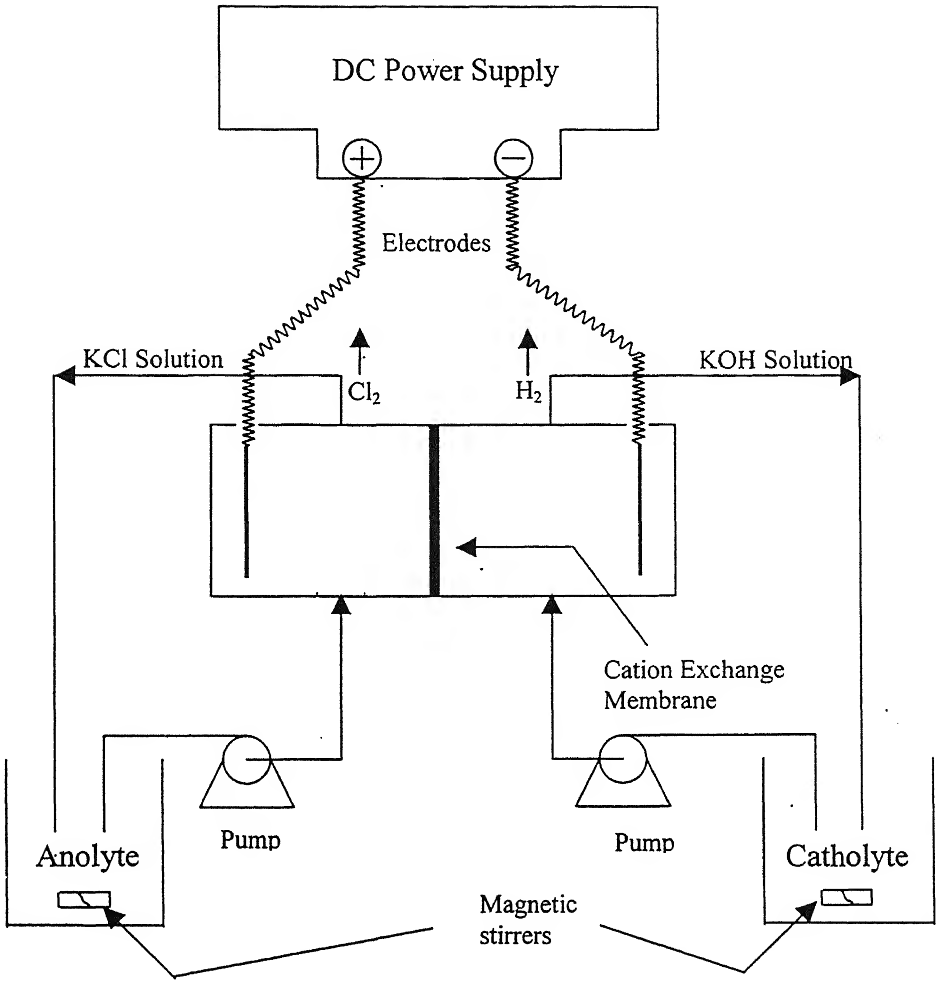

Figure 2.3: Schematic diagram of the Experimental setup used for electrodialysis

Chapter 3

RESULTS AND DISCUSSIONS

3.1 Development of clay supports

For the synthesis of clay supports, various clay materials (as described in Table 2.1) are mixed with distilled water, in the composition specified and made into thick paste. This paste is molded in the form of a circular disc by using shallow stainless steel ring, which is placed over a dry and flat gypsum surface. The drying of the clay supports is carried out in 3 stages as follows:

(a) Air drying under ambient conditions for 24 hours.

(b) Oven drying at 100 ^{0}C for 12 hours.

(c) Oven drying at 250 ^{0}C for 12 hours.

Slow drying of the clay supports is of prime importance and non-uniform, fast or differential drying leads to the development of surface cracks. The gypsum surface also plays an important role during the drying and the supports molded over glass, firebrick or stainless steel surface develop significant cracks. Cracking has been explained to occur because of the following reasons [66]:

(a) Case hardening occurs when shrinkage of surface material has ended, but the internal material with higher liquid content continues to shrink. The development of internal tensile stress as a result of it may produce internal cracks.

(b) Differential shrinkage leads to warping because of non-uniform drying across the thickness.

(c) Cracks develop when surface material becomes brittle.

(d) Mechanical resistant of shrinkage.

(e) Contact friction between firebrick surface and the clay supports leads to surface cracks, which normally occurs if the product is heavy and the support is highly rough.

We have eliminated the surface cracks by the orientation of the supports in stage (b) and (c) of the drying. During oven drying, the clay supports are kept vertically in the grooves cut in firebrick. The firebrick surface, being highly water absorbing, is likely to give a faster driving force for drying than the less porous gypsum surface and hence giving rise to surface cracks.

3.2 The calcining process

After drying in stage 3, the clay supports are calcined in a furnace at 900 ^{0}C for 6-8 hours. It is done to provide the desired mechanical strength to it and the structural changes occurring during this reaction are given below:

(a) The clay particles condense together into a crystalline hard and rigid compact.

(b) Water of kaolin is eliminated between 450 ^{0}C and 700 ^{0}C by the reaction producing metakaolin $Al_2Si_2O_6$.

$$\underset{\text{(kaolin)}}{Al_2Si_2O_5(OH)_4} \longrightarrow \underset{\text{(metakaolin)}}{Al_2Si_2O_6} + 2\,H_2O$$

(c) Dehydration of aluminum hydrates occurs between 320 – 520 ^{0}C.

(d) The organic matter in ball clay is oxidized between 200 – 700 ^{0}C.

(e) Decomposition of calcium carbonate occurs between 200 – 700 ^{0}C.

$$CaCO_3 \longrightarrow CaO + CO_2$$

These gaseous products are expelled during calcination process and produces volume expansion and the formation of pores within the supports. In order to get a good, flat and porous support, the following precautions must be followed:

(a) Complete removal of moisture from the supports prior to calcining process.

(b) By controlled rate of heating in the furnace, thus allowing the gradual removal of gaseous products from the supports.

(c) By vertical orientation of the clay supports during oven drying and calcining.

Complete elimination of the defects appears to be difficult and the surface non-uniformity, thus introduced, is removed by polishing the sintered clay discs on a fine silicon carbide abrasive paper (No. C-220). The water flow, in the clay supports thus prepared, occurs under atmospheric pressure.

3.3 Preparation of Iron salt embedded zeolite clay composite membrane

In order to prepare a zeolite membrane having high current efficiency, we discovered the following three important factors. The first one is the reaction time in a given deposition of Analcime C zeolite in hydrothermal reaction. The second important factor is that a given membrane needed to be compacted by repeated cycles of hydrothermal reactions. Finally, the presence of Fe^{2+} ions (after the compaction of the membrane has been done) makes considerable difference in the current efficiency and energy consumption. These are now systematically discussed below.

The hydrothermal crystallization of the zeolite layer within the mesoporous clay supports has been done in a basic medium and the composition of synthesis gel is given in Table 2.2. Time of the hydrothermal reaction is varied from 3, 6, 12, 24, 48 to 72 h, and

the corresponding cation exchange capacity (CEC) of zeolite powder is given in Table 3.1. The CEC is found to be maximum (1.72 meq/g dried zeolite) for 12 h of the reaction. To make a dense membrane, the zeolite is deposited repeatedly with 12 h reaction and a gain in mass of the support (given in Table 3.2) is observed for all the repetitions. From this table, it can be seen clearly that there is no significant increase in the mass of the support after 6 cycles of depositions. The optimal conditions for the synthesis of zeolite layer are given in Table 3.3. The zeolite membrane prepared under these optimum conditions is subjected to $FeCl_2$ deposition using procedure described in section 2.2.3 and the amount of $FeCl_2$ deposited is 0.03 g. After $FeCl_2$ has been deposited, the deposition of TEOS layer on the surfaces is carried to trap the salt. Figure 3.1 shows the photographs of the clay support, zeolite clay composite membrane and iron salt deposited zeolite clay composite membrane.

3.4 Characterization of the membrane

Membrane material has then been characterized using the XRD analysis of the zeolite powder formed during the hydrothermal crystallization, SEM of the deposited membrane, CEC of the zeolite powder, pore size distribution of the membrane and current-voltage characteristics. These are discussed below one by one.

3.4.1 XRD of zeolite layer deposited within the mesoporous compacts

In order to characterize the structure of the zeolite layer, the powder formed in the autoclave during its synthesis was subjected to XRD analysis (XRD pattern shown in Figure 3.2). The X-Ray wavelength was kept constant at 1.5406 A^0 and the relative

intensity of the diffraction is recorded as the function of 2θ or d spacing. The XRD pattern of the zeolite powder was compared with the patterns given in the JCPDS file and was found to match with the file # 41-1478 [67] which is an Analcime-C zeolite with cubical crystal structure. Table 3.4 gives all the structural parameters of the zeolite along with its chemical formula. The experimental d values of our zeolite powder and that of the matched zeolite are given in Table 3.5.

3.4.2 Scanning electron microscopy (SEM)

SEM is used to characterize the structural morphology of the composite membrane and Figure 3.3 shows the SEM photographs of the zeolite layer. Figure 3.3 (a) is the top view of the membrane and it shows the partial covering of clay support by zeolite crystals. Figure 3.3 (b) shows the top view at higher magnification. Figure 3.4 is the cross-sectional view of the membrane and it shows two distinct layers. It can be seen that the (brighter) zeolite crystals partially fill up the pores of the clay support in the top layer (right side of the photograph) while the bottom layer consists only of the clay particles [50].

3.4.3 Cation exchange capacity

The cation exchange capacity (CEC) of the zeolite powder is determined by procedure discussed in section 2.3.3. The effect of reaction time on CEC is reported in Table 3.1. The optimum time for hydrothermal reaction is found to be 12 hours for which the highest CEC is 1.72 meq/g of the dried zeolite.

3.4.4 Pore size distribution

The Bubble point technique has been chosen, over mercury penetration and nitrogen absorption-desorption techniques, because it distinguishes between the dead end pores and the pores available for permeation and it can differentiate between the pores of thin zeolite layer and the pores of the support [50, 51]. In our case, water is chosen as the wetting liquid and butanol, as the non-wetting liquid due to their large differences in surface tensions. The flow rates of butanol when the pores of the membrane have previously been filled with water and when the pores are empty are plotted against the applied pressure difference (Δp). In the former case the flow rate curves are nonlinear while they are linear for the latter. Figure 3.5 shows the flow-pressure curves of the single cycle deposited zeolite membrane and six cycles deposited zeolite membrane, and from this it is observed that up to a certain Δp, there is no flow (n-butanol) and the wetting liquid (water) acts as a barrier. At higher pressures, the flow rate is found to increase and at a certain pressure, it meets the linear butanol flow rate (when the membrane pores are not filled with water) curve. It is suggested that at this point, all the pores are available for permeation. By using Equation 2.2 and with the knowledge of surface tensions of both fluids and contact angle values, this pressure has been employed to obtain the pore-size range for the membranes. Pore size distribution of the single cycle deposited membrane is found to be 30.0 to 78.0 nm which reduces to 7.3 to 15.1 nm after the final cycles of depositions. Deposition of $FeCl_2$ does not alter the pore size distribution of the membrane.

3.4.5 Current-Voltage curve for the membrane

The metal embedded membrane thus prepared has extremely low current efficiency initially (See Figure 3.6). After placing the membrane in a setup of Fig. 2.2, the cell was operated for two hours at room temperature with the anolyte chamber having KCl solution (concentration 2 N), then it was shutdown for 24 hours and this constituting cycle 1. The next day the membrane was subjected to the second cycle and the average current efficiency over the two hour experiments evaluated. The current efficiency is low initially (about 41%) which improves with number of cycles to a higher value of 88% after eight cycles. This experiment suggests that cations are initially trapped inside giving subsequent improved performance.

The I-V characteristic of a membrane gives the information about the limiting current density for the membrane. Figure 3.7 shows the I-V curve of the compacted (six cycles deposited) zeolite clay composite membrane and metal embedded zeolite clay composite membrane under the same experimental conditions specified in section 2.3.5. It clearly shows that the voltage drop across the compacted zeolite membrane (after activated as in Fig. 3.6) was 1.29 V for zero current density and then increases linearly with increase in the current density. As opposed to this, for iron salt embedded membrane voltage drop was 0.58 V for zero current density and then increased with increase in current density showing a decrease in resistance of membrane at higher applied current density.

3.5 Effect of Operating Conditions on Membrane Performance

The performance of the membrane has been evaluated in terms of current efficiency which is a measure of the fraction of current carried by K^+ ions, and energy consumption. The effect of operating conditions (current density, circulation rates of solutions, salt and alkali concentrations and temperature) on current density and energy consumption has been studied and reported in this section. Simultaneously, these results have been compared with that of sodium chloride solution at different operating variables.

Figure 3.8 shows the variation of the current efficiency for single cycle deposited zeolite clay composite membrane, compacted zeolite clay composite membrane and metal salt embedded zeolite clay composite membrane with time. This figure clearly shows that the current efficiency is higher for six cycle compacted membrane and even higher for the metal embedded membrane compared to that for one time deposited zeolite clay composite membrane. Experiments for the pore size distribution (as shown in Figure 3.5) show that the pore size reduced during various cycles of compaction. However the metal deposition does not alter the pore size and increase in current efficiency. In reference 68, the enhancement of water splitting using the bipolar membrane was explained through increase in hydrophilicity of the membrane due to $Fe(OH)_3$ formation. In our case the Fe^{2+} ions in the membrane may have been present in the hydrated form this way increasing its hydrophilicity and current efficiency. It also shows that the current efficiency slightly decreases with time for the membranes, which is likely to be deposition of salts on the membrane surface as reaction proceeds, this way giving concentration polarization.

Table 3.6 shows the variation of voltage drop with time for the three membranes. It is clearly seen that the voltage drop is slightly decreased with time for all three

membranes because as reaction proceeds, the K^+ concentration in catholyte chamber increases, increasing the conductivity. Also the voltage drop is higher for compacted zeolite membrane because of reduced pore size and for the iron salt embedded membrane is lower than for the compacted zeolite membrane without metal deposition because of increase in conductivity of the membrane in presence of metal salt inside the pores.

Because of higher current efficiency and lower voltage drop for the iron salt embedded membrane, we did all the experiments with the iron salt embedded membrane. The effect of current densities on current efficiency for the metal salt embedded zeolite clay composite membrane is plotted in Figure 3.9 at the circulation rates of 33 ml/min, salt concentration of KCl 2.0 N and initial KOH concentration of 0.2 N. A decrease in current efficiency was observed at higher current densities, especially at 509.2 A/m^2. The trend is same as reported earlier by Tzanetakis et al. [33] indicating that the higher current densities might have been above limiting current, although this was not evident from I-V curve (see Figure 3.7). The cell voltage and energy consumption is reported in Table 3.7 (Run 1, 2 & 3) which shows that the amount of energy required per mole of KOH produced increase with increase in current density because of higher cell voltage and lower current efficiency at higher current densities. On comparing these results with NaCl solution (Figure 3.9), it can be seen that NaCl gives better efficiency. It may be because at higher current density, more sodium ion passes through membrane than potassium ion.

It is clear from the Figure 3.10 that the current efficiency improves when the potassium ion content in the feed was increased, and thus the salt concentration ideally should be as high as possible [33]. Because of higher current efficiency, energy consumption is lower for higher salt concentrations as shown in Table 3.7 (Run 2, 6 & 7).

Comparing its results with that of NaCl solution (Figure 3.10), it is seen that KCl solution gives better efficiency than NaCl solution. It is because ionic radius of potassium ion in water is smaller than that of sodium ion in water [69]. So at higher salt concentration, potassium ion passes easily through membrane than sodium ion.

The influence of flow rates on current efficiency for metal salt embedded membrane is presented in Figure 3.11 which shows that the current efficiency slightly decreases at higher flow rates. This may have been due to the transport behavior associated with gas evolution is not the rate limiting step in the narrow cell channel at the low flow rate [33]. This leads to a slight increase in energy requirements with increase in flow rates as shown in Table 3.7 (Run 2, 4 & 5). As shown in Figure 3.11, flow rate does not affect current efficiency of sodium or potassium salt solution considerably.

As we increase the KOH concentration in catholite compartment, the current efficiency slightly goes down which can be seen from Figure 3.12, and the voltage drop across the cell decreases due to the increased conductivity of the solution, and as a combined result, energy consumption is almost constant as seen in Table 3.7 (Run 2, 8 & 9). Comparing these results with NaCl solution (Figure 3.12), it is found that sodium salt solution gives better current efficiency than potassium salt solution. This may be because electropositive character of potassium is more than that of sodium. So at higher base concentrations, less potassium ions will come to catholyte chamber than sodium ion giving lower efficiency.

The effect of temperature was studied at current density of 254.6 A/m^2, flow rate of 33 ml/min, salt concentration of 2.0 N and initial KOH concentration of 0.2 N, and the results are shown in Figure 3.13. As we increased the temperature from 30 to 70 ^0C,

current efficiency increased from 88 to 96% and as the cells made were made of Perspex, we could not study performance at higher temperature. Higher temperatures give an increase in diffusivity of K^+ ions and thus increase the selectivity of membrane for K^+ [34]. The voltage drop and energy consumption data for all temperatures are reported in Table 3.7 (Run 2, 10 & 11) which shows that as we increase the temperature, cell voltage decreases for the same current density and as combined effect of current efficiency and cell voltage, energy consumption decreases by noticeable amount. As compared to the results for NaCl solution in Figure 3.13, it can be seen that current efficiency for potassium salt solution is better than in sodium salt solution. It is because at higher temperature, more potassium ion can diffuse through membrane than sodium ion because of its less ionic radii in water.

The overall performance of the iron salt embedded zeolite clay composite membrane is summarized in Table 3.7. Table 3.8 shows the comparison of the current efficiency, voltage drop and energy consumption of compacted zeolite clay composite membrane and iron salt embedded zeolite clay composite membrane with Nafion®, RAI and RAI-N membranes. This Table clearly shows that the metal salt embedded membrane giving better performance at room temperature in terms of current efficiency and energy consumption to that of the membranes reported in the literature [33, 44, 70 & 71].

Table 3.1: Cation exchange capacity (CEC) as a function of hydrothermal reaction time

Hydrothermal Reaction Time (Hour)	**CEC (meq/g dried zeolite)**
3	0.85
6	1.09
12	1.72
24	1.49
48	1.34
72	1.33

Table 3.2: Gain in mass of clay support after deposition of zeolite with repeated depositions

No. of deposition	**Wt. before zeolite deposition (g)**	**Wt. after zeolite deposition (g)**	**Gain in wt. (g)**
1^{st}	9.73	10.99	1.26
2^{nd}	10.99	11.88	0.89
3^{rd}	11.88	12.37	0.49
4^{th}	12.37	12.65	0.28
5^{th}	12.65	12.80	0.15
6^{th}	12.80	12.88	0.08

Table 3.3: Optimal conditions for the synthesis of zeolite layer

Parameter	**Optimum Values**
Hydrothermal crystallization temperature (^{0}C)	200
Crystallization time (h)	12
Pressure attained (psi)	Autogeneous
Deposition repeated	6 times

Table 3.4: Crystal structure data of zeolite

Property	**Value**
Crystal geometry	Cubic
Chemical formula	$Na(Si_2Al)O_6.H_2O$
Lattice parameter	a = 13.7067 A^0
Molecular weight	220

Table 3.5: Analysis of XRD pattern of Analcime-C zeolite

% Intensity of Fig. 3.2	d (A^0) of Fig. 3.2	d (A^0) of JCPDS file # 41-1478	hkl from file # 41-1478
44.82	5.6293	5.5900	211
16.32	4.8696	4.8437	220
10.59	3.6840	3.6670	321
100	3.4477	3.4254	400
59.22	2.9407	2.9209	332
10.51	2.8113	2.7970	422
19.95	2.7049	2.6874	431
21.77	2.5189	2.5006	521
10.45	2.4371	2.4230	440
12.97	2.2355	2.2222	611
5.66	2.0315	2.0204	631
20.49	1.9132	1.9375	543
13.26	1.8783	1.8652	721
26.50	1.7515	1.7406	651
10.63	1.7242	1.7127	800
12.78	1.6949	1.6868	741
6.25	1.6710	1.6611	820
5.45	1.6226	1.6150	660
10.29	1.6009	1.5933	831
6.00	1.5016	1.4953	842
8.63	1.4845	1.4775	921
4.89	1.4506	1.4619	664
12.08	1.4194	1.4136	932
7.57	1.3765	1.3707	860
15.39	1.3618	1.3569	772
7.59	1.3111	1.3065	1031
6.59	1.2882	1.2836	871
6.28	1.2657	1.2615	961
9.69	1.2247	1.2209	963

Table 3.6: Cell voltage for iron salt embedded membrane and membranes without iron salt (Current density = 254.6 A/m^2, Flow = 33 ml/min, Salt = 2.0 N, Initial KOH Conc. = 0.2 N, Temp. = 30^0C)

Time (min)	Cell Voltage for single cycle zeolite clay composite membrane (V)	Cell Voltage for compacted zeolite clay composite membrane (V)	Cell Voltage for iron salt embedded zeolite clay composite membrane (V)
0	4.8	6.7	5.6
30	4.8	6.6	5.6
60	4.7	6.6	5.5
90	4.6	6.5	5.5
120	4.6	6.5	5.5
150	4.5	6.4	5.4

Table 3.7: Overall performance of the iron salt embedded zeolite clay composite membrane

Run	Flow Rate (ml/min)	Current Density (A/m^2)	KCl (N)	Initial KOH Conc. (N)	Temperature (^0C)	Cell Voltage (V)	Current Efficiency (%)	Energy Consumption (kWh/mol KOH)
1	33	127.3	2.0	0.2	30	4.33	89.4	0.1489
2	33	254.6	2.0	0.2	30	5.58	87.6	0.2030
3	33	509.2	2.0	0.2	30	8.03	66.1	0.4137
4	100	254.6	2.0	0.2	30	5.73	85.8	0.2095
5	165	254.6	2.0	0.2	30	5.80	84.0	0.2122
6	33	254.6	1.5	0.2	30	5.85	76.8	0.3089
7	33	254.6	3.0	0.2	30	5.20	89.4	0.1849
8	33	254.6	2.0	0.1	30	6.49	95.6	0.2172
9	33	254.6	2.0	0.5	30	5.01	84.9	0.1928
10	33	254.6	2.0	0.2	50	4.99	92.9	0.1584
11	33	254.6	2.0	0.2	70	4.55	96.5	0.1399

Table 3.8: Comparison of the performance of iron salt embedded zeolite clay composite membrane with Nafion 117®, RAI and RAI-N membranes at room temperature [33, 34 and 71]

Membrane	Voltage drop (V)	Current Efficiency (%)	Energy Consumption (kWh/mol KOH)
Compacted zeolite clay Composite membrane	6.6	68.6	0.2920
Iron salt embedded zeolite clay Composite membrane	4.3	89.4	0.1489
Nafion 117® membrane*	4.6	78.0	0.1581
RAI membrane	4.9	48.5	0.2852
RAI-N1 membrane	4.9	53.4	0.2400
RAI-N2 membrane	4.9	70.9	0.1880

* Voltage drop for Nafion® taken from reference 71 and current efficiency from reference 33. The energy consumption was calculated using these under same operating conditions.

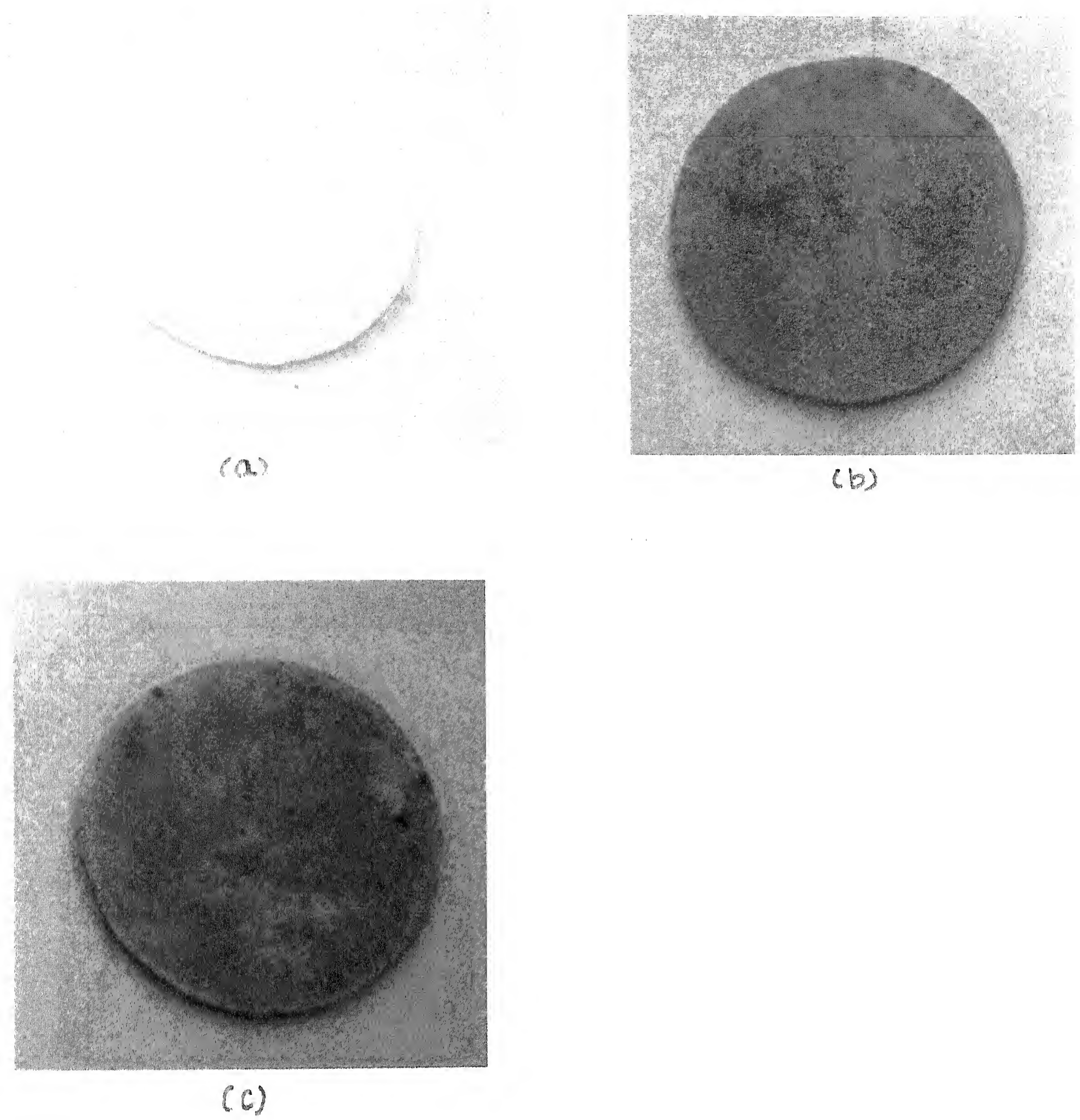

Figure 3.1: Photographs showing the membrane during different stages (a) clay support, (b) zeolite clay composite membrane and (c) iron salt embedded zeolite clay composite membrane

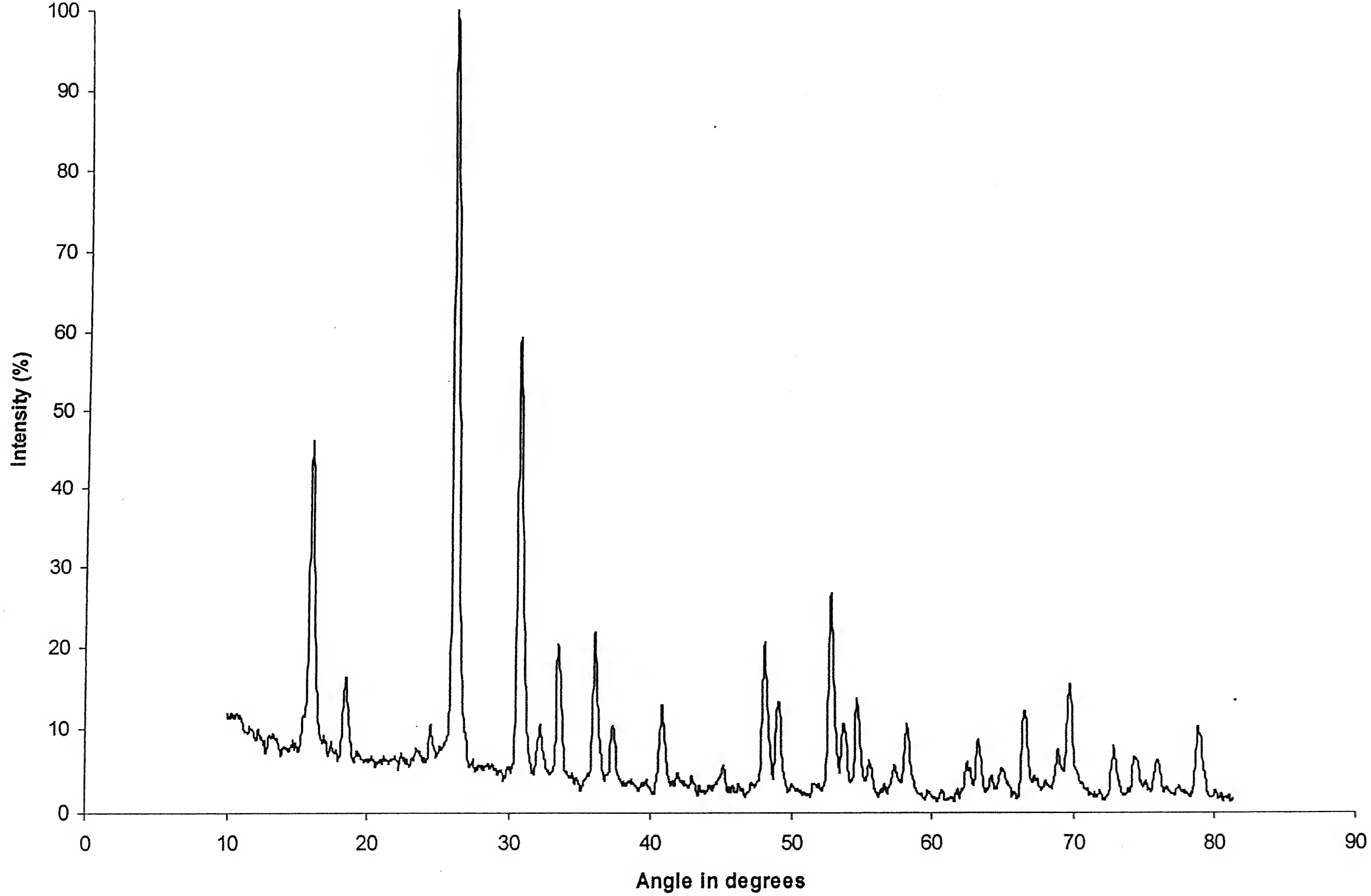

Figure 3.2: XRD pattern of Analcime-C zeolite powder formed during hydrothermal crystallization reaction

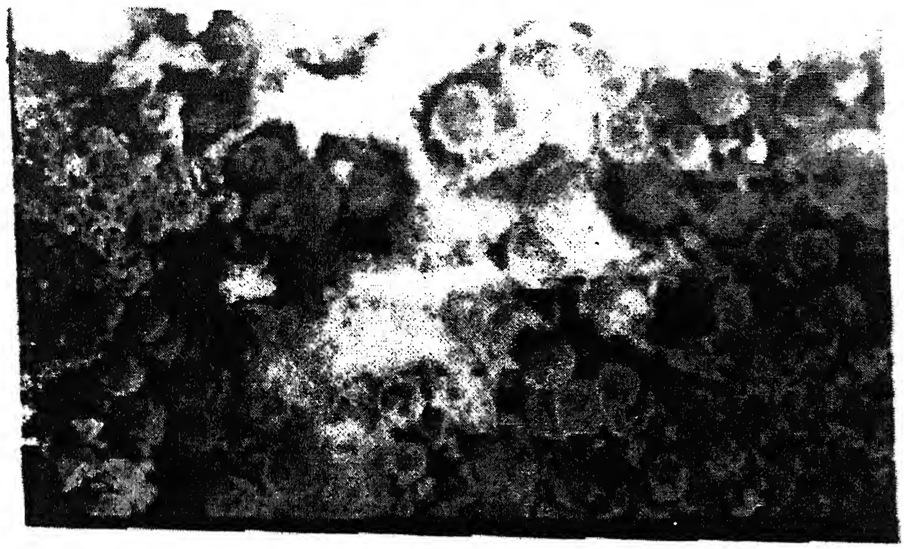

10 μm
(a) Magnification: 250

10 μm
(b) Magnification: 700

Figure 3.3: SEM photograph showing the top view of the membrane at two different magnifications. The bright layer in photograph (a) is the zeolite layer formed over the clay support. Photograph (b) shows the area at a higher magnification where the zeolite particles can be distinctly seen on the top left of the photograph while the bigger size particles are that of clay

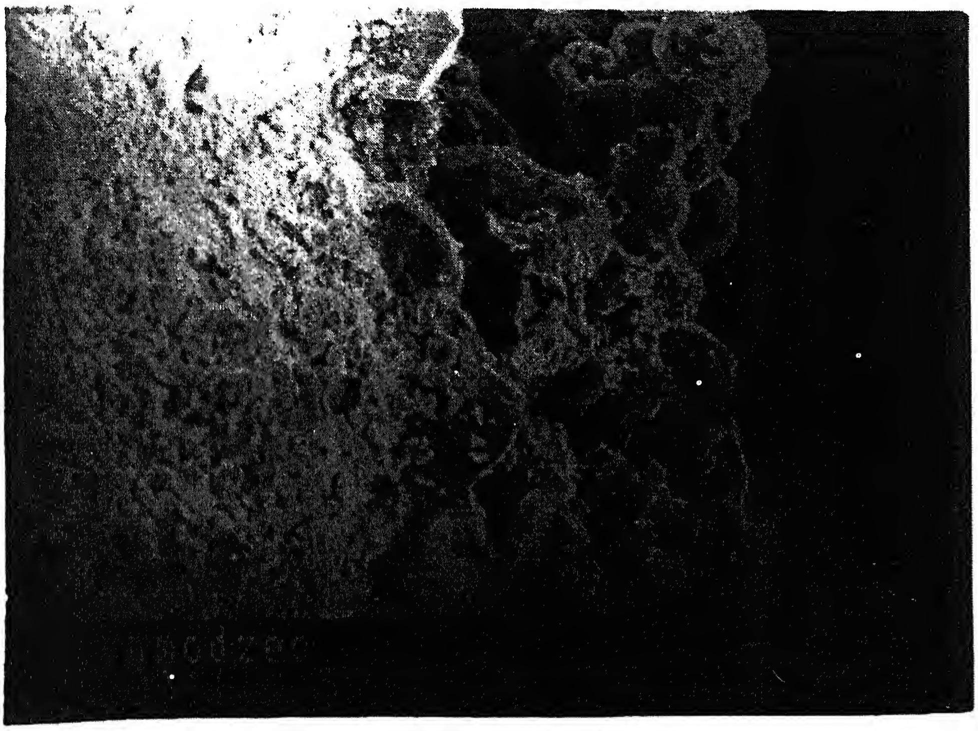

Figure 3.4: SEM photograph showing the cross-sectional view of the membrane. The bright layer at the left side of the photograph represents the part of support whose pores have been partially filled up by the zeolite crystal while the right side shows the bigger clay particles

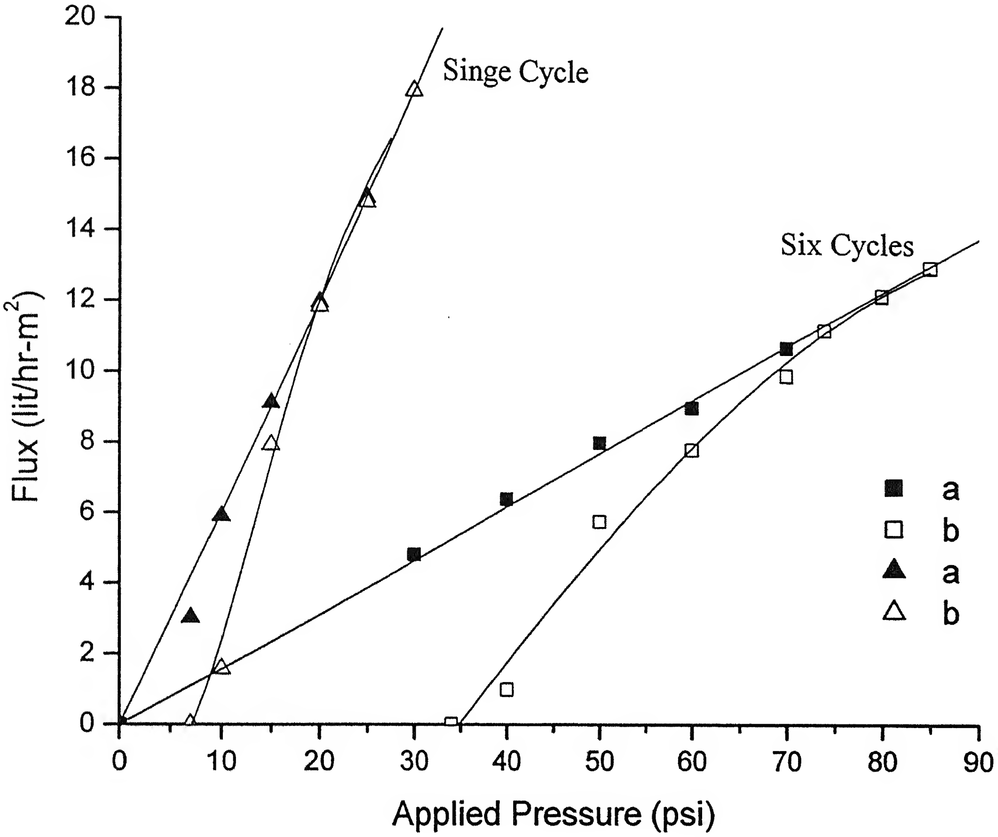

Figure 3.5: Flux -pressure curves for single cycle and six cycle deposited zeolite clay composite membranes. a) Butanol Flux b) Butanol Flux when membrane pores are filled with water

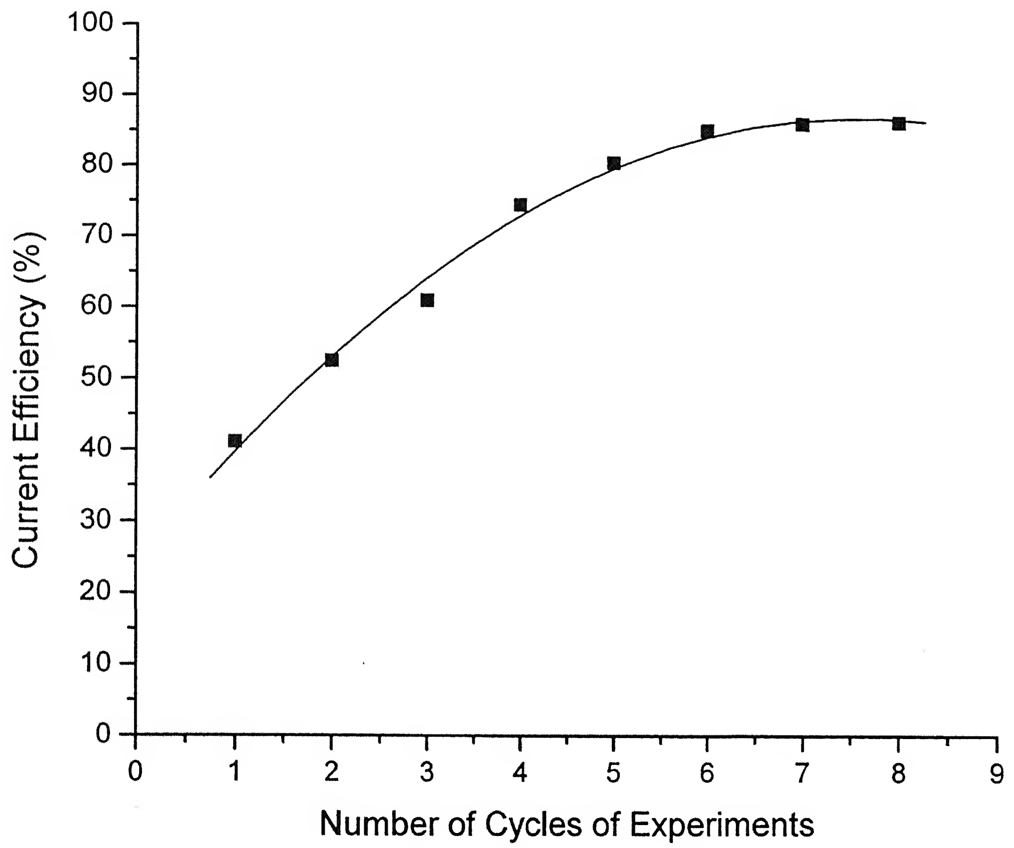

Figure 3.6: Current efficiency of a new membrane vs. the number of cycles of experiments that it has been exposed to. One cycle of experiment is defined as two hours of electrodialysis of KCl with 24 hours of shutdown.

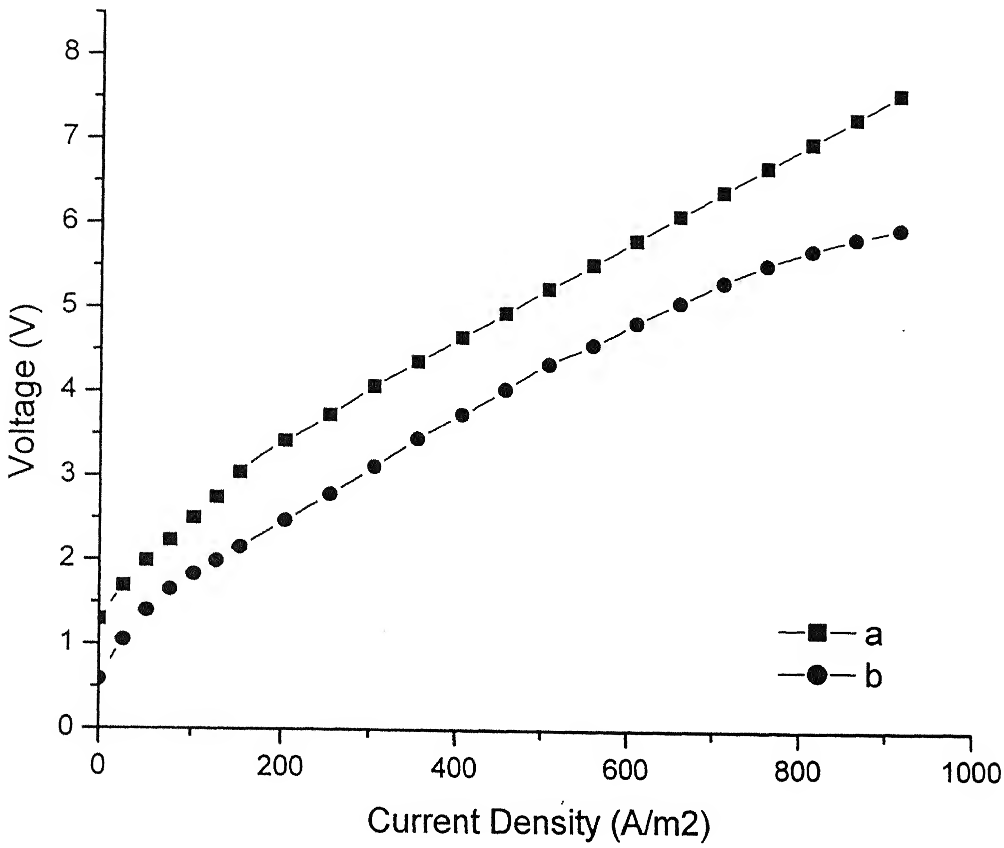

Figure3.7: *I-V* characteristics of the membranes. a) compacted zeolite clay composite membrane, b) iron salt embedded zeolite clay composite membrane

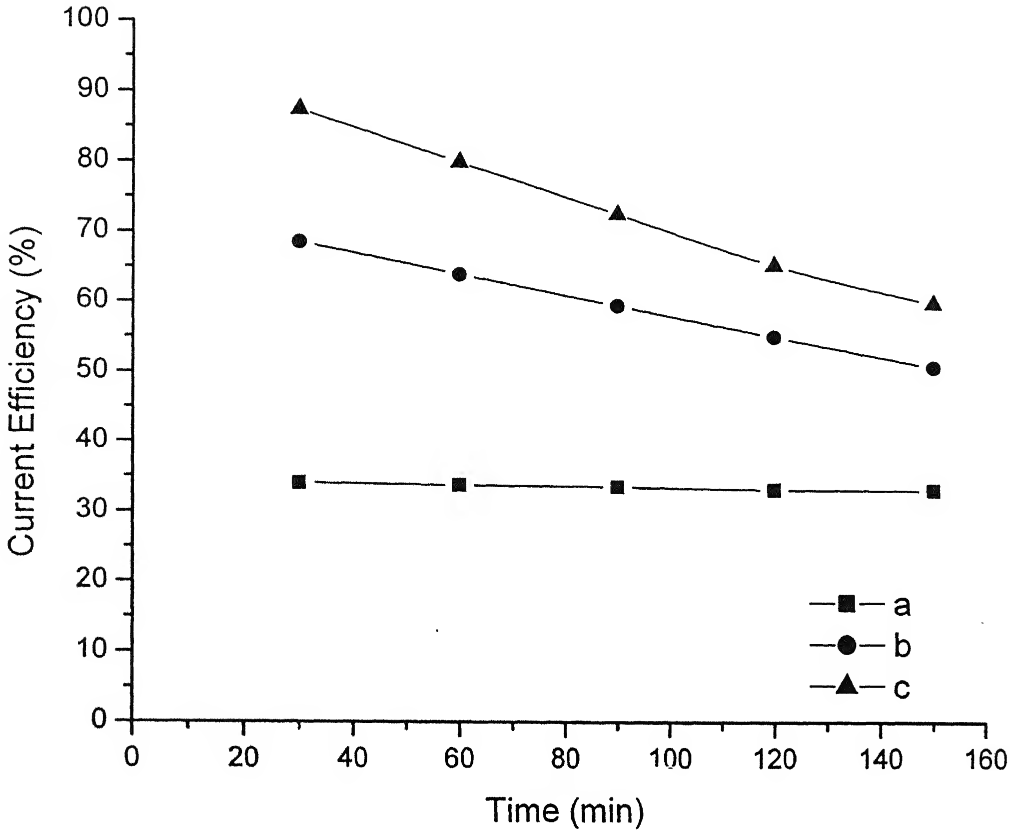

Figure 3.8: Variation of current efficiencies with time at Current density = 254.6 A/m^2, KOH Conc. = 0.2N, Flow = 33 ml/min, Salt = 2.0 N, Temp. = 30 ^{0}C. a) single cycled zeolite clay composite membrane, b) six cycled zeolite clay composite membrane and c) iron salt embedded six cycled zeolite clay composite membrane

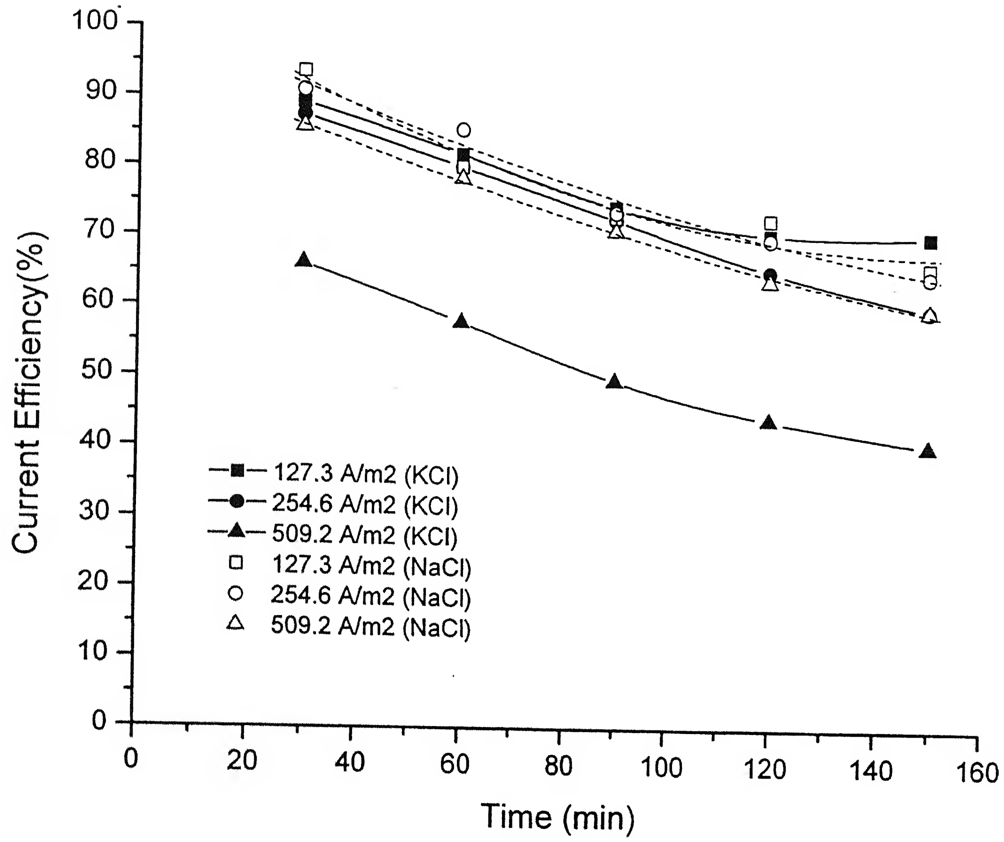

Figure 3.9: Variation of current efficiencies for iron salt embedded membrane with time at different Current densities (Flow = 33 ml/min, Salt conc. = 2.0 N, Temp. = 30 ^{0}C, Initial base conc. = 0.2 N)

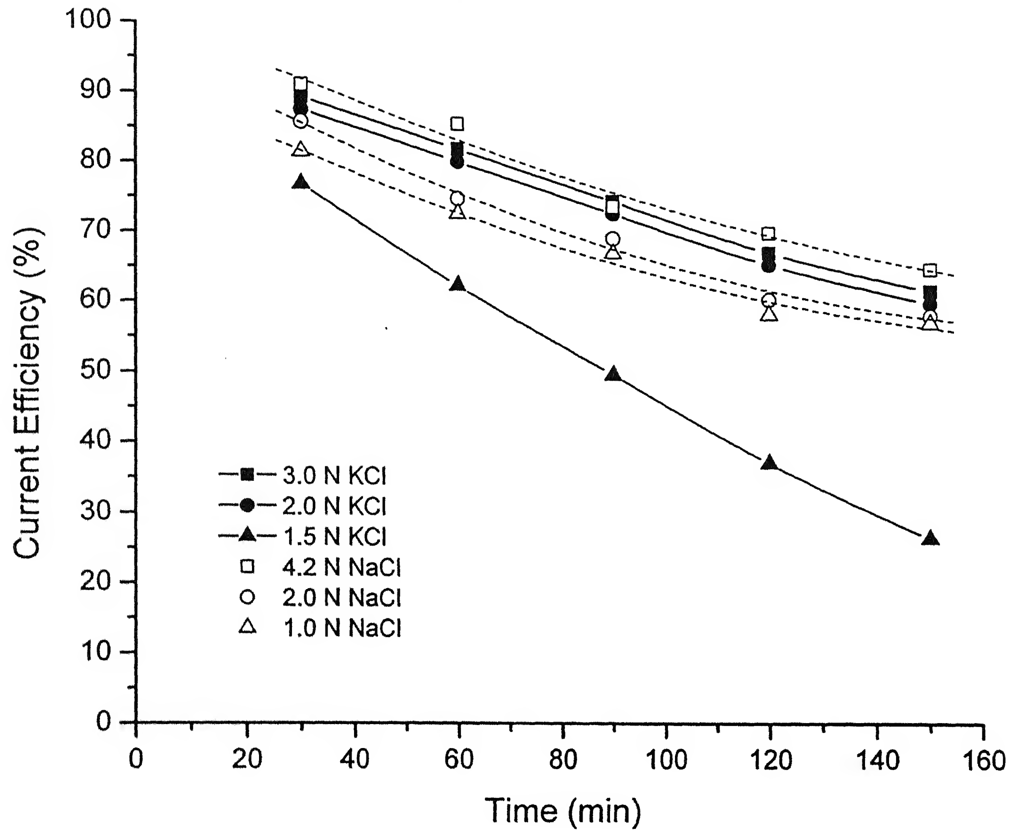

Figure 3.10: Variation of current efficiencies for iron salt embedded membrane with time at different salt concentrations (Current density = 254.6 A/m^2, Flow rate = 33 ml/min, Initial base Conc. = 0.2 N, Temp. = 30 ^{0}C)

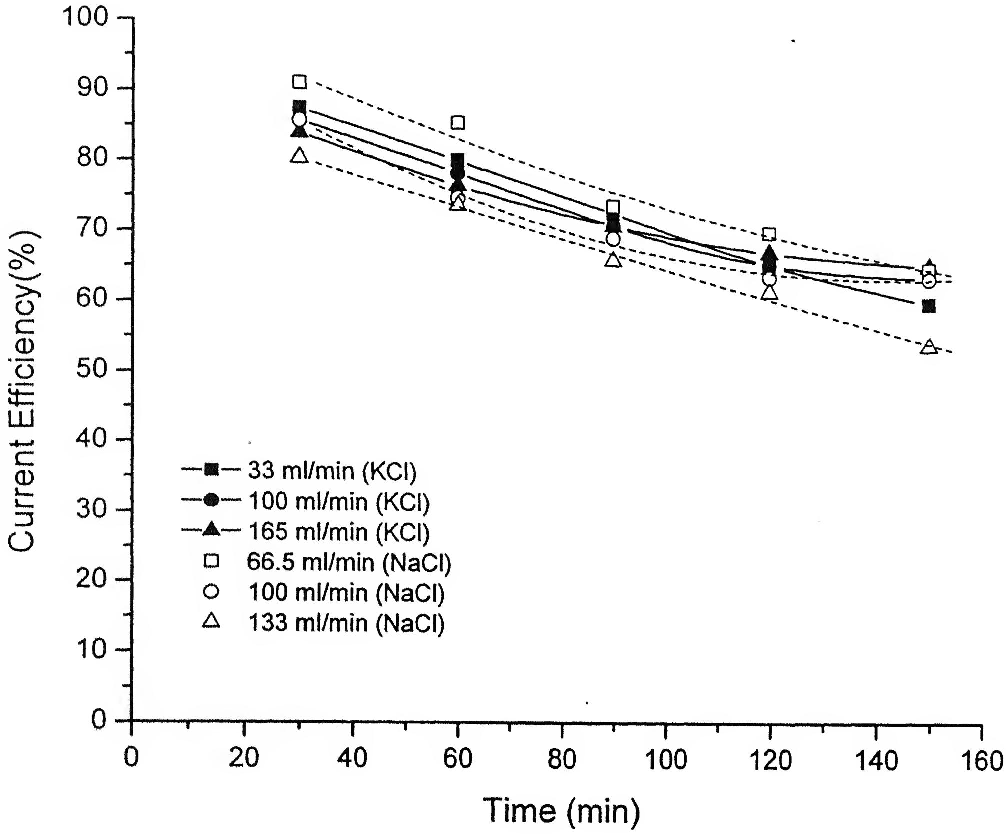

Figure 3.11: Variation of current efficiencies for iron salt embedded membrane with time at different circulation rates of catholyte and anolyte solutions (Initial base Conc. = 0.2 N, Salt conc. = 2.0 N, current density = 254.6 A/m^2, Temp. = 30 ^{0}C)

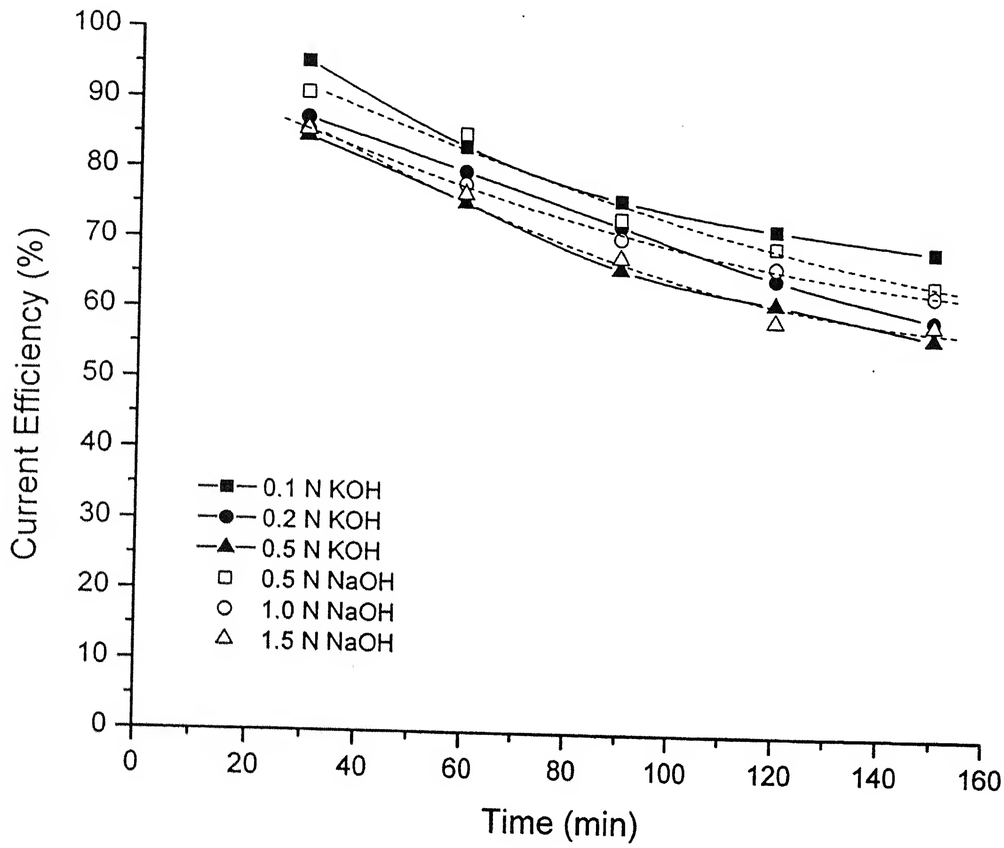

Fig. 3.12: Variation of current efficiencies for iron salt embedded membrane with time at different Initial base concentrations (current density = 254.6 A/m^2, flow rate = 33 ml/min, Salt conc. = 2.0 N, Temp. = 30 ^{0}C)

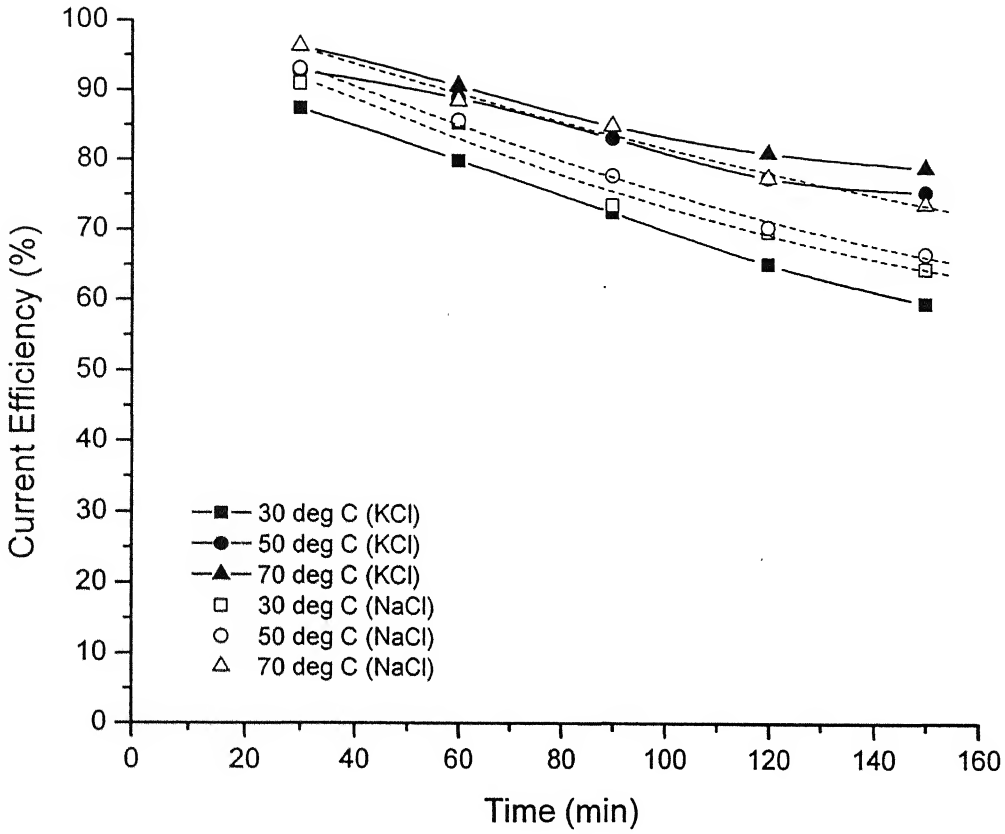

Figure 3.13: Variation of current efficiencies for metal embedded membrane with time at different Temperatures (Current density = 254.6 A/m^2, flow rate = 33 ml/min, Salt conc. = 2.0 N, initial base Conc. = 0.2 N)

Chapter 4

SCALE-UP EXPERIMENTS OF NITRATION OF PS-DVB AND PMMA-EGDM RESINS

After completing my work on cation exchange membrane, I decided to work on the scale up of laboratory scale experiments on nitration of PS-DVB and PMMA-EGDM resins. Experiments have already been reported on laboratory scale (1.5 g in one time reaction) nitration of resin using a 2.5 liter bottle reactor [72] and I have scaled up the reactor carrying out nitration of 66 g resin in 40 liter reactor.

The experimental setup for nitration of resin (PS-DVB and PMMA-EGDM copolymer resin) based on laboratory scale studies (see Tables 4.1 and 4.2) [72] was designed and provided by Jubilant Organosys Ltd., Gaziabad (shown in Figure 4.1). It has a two-way compressor which on proper closing of valve sequences can produce vacuum (closing the valves A, B & D and opening C & E) as well as pressure (closing the valves B & E and opening A, C & D) within the reactor. In order to introduce NO_x into the reactor, the entire reactor was first evacuated and the gas was introduced. After this sufficient oxygen was introduced which increased the reactor pressure by a factor of two. When the temperature was increased to 120^0 C, the gas became highly corrosive and within the reactor, there was considerable amount of nitric acid causing acid rain.

A known amount of resin was needed to be introduced into the reactor, but could not be done so easily because the reactor was just a hollow tube. We solved this problem, we hanged a stainless wire mesh and the resin was placed on it. Somehow in this setup, the amount of moisture getting in could not be stopped and due to the acid rain (of nitric acid), the resin were completely destroyed and formed a pulp in a liquid. Since the valves

were made of brass, they were constantly corroded by NO_x, requiring replacements (we replaced it five times). Eventually the compressor developed a leak which could not be rectified. In view of absence of sustained pressure or vacuum, the system had to be abandoned.

Once the reactor was judged to be unsuitable, we decided to nitrate the resin in 40 liter drum (Φ 34 cm, H 44 cm) sealed from the top with a lid screwed on it. This assembly was made of cast iron which quickly formed rust due to the reaction with NO_x filled into it. We have following three characteristics dimensions in the nitration experiments:

1. Volume of resin V_R
2. Volume of gas V_{NO2}
3. Volume of the drum V_D

There are two volume ratios (V_R/V_{NO2}) and (V_{NO2}/V_D) and they serve the basis of the scale up. On reading the procedure of nitration given in Table 4.1 and 4.2, it appears that we need about 300 ml. of NO_x and 300 ml. of O_2 for every one gram of resin. So we decided to put 1.5 Kg. of resin in the drum and supply 900 liter ($600 x 1.5 x 10^3$ ml.) of gas in a 40 liter drum in 23 sequential iterations with nitration time of 7 hours each (Run 1; Table 4.3).

On doing nitration experiments as described above, we found that the resin particles continued to absorb NO_x and we could react as much as 700 ml/g of resin and the colour of the resin changed to bright red. However, on immersing the resin in toluene and keeping it for overnight, red coloured fluid soluble in toluene comes out leaving the lightly nitrated resin. This indicates that the nitration reaction time beyond seven hours appear to produce degradation products in excess, this way limiting the utility of this

procedure. This experiment reveals that the total nitration time is a very important parameter and cannot be more than seven hours. It is thus seen that if the volume of the drum is 40 liter, assuming that about 300 ml of NO_x per gram of resin is required, the total amount of resin that should be used for the nitration reaction is $\frac{20lit}{0.3lit/g}$ or 66.7 g.

Next important task in designing the tank was deciding the material of construction. We observed that mild steel and cast iron reacted with the NO_x at the reaction temperature. There was rust formation as a result of this and it came out on cleaning the reactors. Since the gas reacted with the material of construction, the lesser amount remained for the reaction with the resin. The NO_x reacted with stainless steel (18/8 SS) also, but did so very slowly. Experiments, on repeated basis, showed that aluminium did not react with the NO_x. We then prepared two mild steel drums (Figure 4.2 showing it schematically) and we passivated its surface in following two way. In the first technique, the inner wall of the drum was painted with aluminium paint and while it was wet, aluminium foil was spread over it. The latter got stuck on the surface and the drum, after overnight drying was baked in oven at 200^0 C for another twelve hours. This particular reactor was filled with NO_x under pressure and was shown to loose NO_x negligibly in an oven for 12 hours at the reaction temperature (Run 16; Table 4.3). Similarly the mild steel drum cladded with thin aluminium (1/20 inch thick) sheet was shown to retain the pressure of the NO_x in twelve hours (Run 17; Table 4.3). It may be recalled that in laboratory scale experiments involving 1.5 g resin were performed in 2.5 liter glass bottle in which NO_x is completely available for reaction, since glass is not affected by it (Run 5-10; Table 4.3). On the commercial level, glass cladded reactors are

difficult to manage and is expensive and aluminium as a material for cladding offers an interesting alternative.

Suppose 2.5 liter bottle is kept in an oven at temperature 130^0C (or 403K) with a syringe needle introduced into the septum. This would mean that the pressure inside bottle is 1 atm and the total moles inside it is [1x2.5/(0.082x403)] 0.076 moles. The bottle is now closed when the syringe needle is removed and is allowed to cool to the room temperature (assumed to be 30^0 or 303K). After cooling, the pressure inside the bottle falls and reaches a value p_{403} x (303/403) or 0.752 atm. Since air consists of N_2 and O_2 in the ratio of 0.79:0.21, the moles of N_2 and O_2 are 0.059 and 0.017 moles respectively. Now in this bottle, 450 ml (or 0.018 moles) of NO_x and 450 ml (0.018 moles) of O_2 are introduced. The total moles of gas in the bottle is now (0.036+0.076) 0.112 moles and the pressure of the gas at 403 K is (0.082 x 0.112 x 403 / 2.5) 1.48 atm. To verify this experimentally, we heated the 2.5 liter bottle in the oven at 130^0 C with syringe needle in the septum. We removed the syringe needle, cooled the bottle outside and measured the vacuum inside the bottle to be 2-3 cm. Hg. We then filled the bottle with NO_x and O_2 and found the pressure to rise up to 7-8 cm. Hg. On heating this gas mixture in the oven at 130^0 C, we found the pressure to be 28-30 cm.Hg or 1.39 atm. which is almost the same as calculated (Run 13, 14; Table 4.3). It is thus seen that ideal gas assumption is justified and the reactor pressure is above 1 atm. Repeated experiments have shown that for the nitration reaction to go smoothly, it is important that the reactor pressure is about 8cm. Hg before putting in an oven. It should also not be above 15 cm. Hg because for pressures above this, there is a possibility of an acid rain formation (Run 15; Table 4.3).

It is also possible that the drum could be evacuated using a strong vacuum pump. Until now the vacuum was created by heating and cooling cycle and is found not to work for a drum of this size. This is because the volume of the drum is much larger than 2.5 liter and the draining of the air through heating-cooling cycle is very slow. As a result of this, the system rarely comes to a thermal equilibrium and the pressure in the tank after one heating-cooling cycle does not change significantly. In view of this the vacuum inside the tank was pulled by an efficient pump and a full vacuum develops within half an hour. After filling the gas (at the rate of 300 ml/g gas and 66 g of resin), the drum pressure is around 1 atm and the pressure at the reaction temperature is considerably smaller than the optimal value. The total gas consumed can be determined by measuring the initial and final pressures. Experiments show that a minimum of 12 cm. Hg after gas filling is required for good nitration. In view of this, in any given nitration reaction, pressure above this can be achieved by filling more gas than that obtained by maintaining 300 ml/g of resin.

The scientific studies on nitration (see Tables 4.1 and 4.2) have shown that the reaction temperature of the resin is the single most important parameter. It has been shown that 10^0 C above the optimum temperature degrades (or burns) the resin and 10^0 C below it almost quenches the reaction. In view of this, the first thing done was modifying the heating arrangement within the oven. Heating coils were placed on all sides and the bottom of the oven so that uniform heating was obtained. Then we argued that the bottle plate temperature must be higher than the average oven temperature (at the centre) which means that within the drum, if resin is placed at the bottom of the drum, it would be burned. Experiments showed that there were at least 20^0 C difference and to overcome this

problem, we proposed to place an asbestos plate between the bottom plate of the oven and the drum. This, however, cut down the heating at the bottom and nitration reaction did not occur at all. So the asbestos plate was removed and the resin was placed in a glass plate and the latter introduced into the drum. In addition there was a fundamental issue whether the temperature control should be done based on the oven temperature or the reactor temperature. So we introduced a thermocouple well in the drum (Figure 4.2) and measured the inside reactor temperature (just above resin glass plate). We were surprised by a temperature difference of 40^0 C between inside and outside and we controlled the oven temperature by measuring the one in the thermocouple well (Run 11, 12; Table 4.3).

Lastly, the literature scheme reported in Tables 4.1 and 4.2 used NO_x generated in a two neck conical flask by H_2SO_4 on a mixture $FeSO_4$ and $NaNO_2$. After complete reaction, for additional NO_x, the latter is added first and then H_2SO_4 is added to it. The role of $FeSO_4$ is to ensure the formation of NO which is present in NO_x. Since $FeSO_4$ is not likely to be affected by H_2SO_4 it was thought that by introducing it once is enough and for additional generation of NO_x one may add only $NaNO_2$ for the action of more H_2SO_4. One can also think of adding the mixture of $FeSO_4$ and $NaNO_2$ for more NO_x. Since O_2 is added in equimolal amount, it was also felt that in its presence, the NO of the NO_x may not really have any role. So we carried out the following three experiments: (a) one in which NO_x was generated by a mixture of $FeSO_4$ and $NaNO_2$ (Run 2; Table 4.3) (b) one in which $FeSO_4$ was added once only (Run 3; Table 4.3) and (c) one in which $FeSO_4$ was not added at all (Run 4; Table 4.3). The results showed that the exchange capacities were not significantly different for these cases.

Table 4.1: Experimental procedure on laboratory scale (1.5 g): Preparation of PS-DVB resin

Step A: Gas Phase Nitration of PS-DVB Resins using NO_x

Direct gas phase nitration of polystyrene-divinylbenzene (PS-DVB) resin occurs extremely efficiently in the presence of small amounts of NO, and is carried out in 2.5 liter reaction bottle. This reaction vessel is equipped with an aluminium cap with a 1.2 mm opening at the top for injecting the gas, which is closed by a silicon rubber septum. A mixture of NO and NO_2 (called NO_x) is generated in a 1.5 liter, two-neck round bottom flask by reacting sodium nitrite $NaNO_2$ (10g, 0.15 mol) with sulfuric acid (H_2SO_4 sp. gr. 1.18, 25 ml) in the presence of ferrous sulfate $FeSO_4$ (5 g, 0.03 mol). The flask is equipped with a rubber septum for withdrawing NO_x, and the gas is withdrawn with the help of a 100 ml syringe.

Approximately 1.5 g of PS-DVB resins are introduced into the reaction vessel and are placed in an oven maintained at the desired reaction temperature. A small needle is punctured through the silicon septum of the reactor vessel so as to allow a thermal equilibrium with the oven. The gas inside the bottle expands due to heating, and escapes through the needle. After this, the needle is removed; the vessel is taken out and allowed to cool at room temperature. This creates a slight vacuum inside the vessel so that when NO_x is introduced into the bottle, at the reaction temperature, the total pressure remains approximately at 1 atm. After feeding the required amount of gas mixture, the vessel is again kept in an oven maintained at the

reaction temperature. After completion of nitration the vessel is taken out from the oven and allowed to cool to room temperature for withdrawing the resin for analysis. If one repeat unit of the unmodified resin is represented by R_1, the overall nitration reaction process can be schematically written as:

$$\text{Ⓟ}CH_2CHC_6H_5 \xrightarrow{NO_x} \text{Ⓟ}CH_2CHC_6H_4NO_2$$

R_1 $\qquad$ R_2

Step B: Amination of Nitrated R_2 Resin

Amination of the nitrated R_2 resin is carried out with hydrazine hydrate as follows: 1.5 g of R_2 resin is placed in a conical flask with 50 ml of hydrazine hydrate and the reaction mass is refluxed at 60^0 C for 4 h in an oil bath maintained at about 60^0 C. After refluxing is over, the resin is filtered, then properly washed with distilled water and dried. These aminated R_3 resin is formed through following reaction and is ready for further processing.

$$\text{Ⓟ}-CH_2CHC_6H_4NO_2 \xrightarrow{\text{hydrazine}} \text{Ⓟ}-CH_2CHC_6H_4NH_2$$

R_2 $\qquad$ R_3

Step C: Modification of Aminated PS-DVB Beads with Dichloroethane

Approximately 1.5 g of R_3 is refluxed with 50 ml 2% v/v solution of dichloroethane in ethanol for 4 h. After the completion of the reaction, the resin is filtered, washed and dried. Higher concentrations of dichloroethane

are avoided because the resin becomes sticky and lumps are formed. No visible change in color is observed, and the reaction occurs as follows:

$$\text{Ⓟ}-CH_2CHC_6H_4NH_2 \xrightarrow{ClCH_2CH_2Cl} \text{Ⓟ}-CH_2CHC_6H_4N(CH_2CH_2Cl)_2$$

R_3 $\qquad\qquad$ R_6

Now this R_6 resin can be easily quarternized with trimethylamine (TMA), triethylamine (TEA) and triphenylphosphine (TPP) as described below.

Step D: Modification of Chloroethylated-Treated R_6, with Trimethylamine, Triethylamine and Triphenylphosphine

After modification with dichloroethane, the dried R_6 resin is treated with 20 ml of 5% v/v trimethylamine in ethanol and the entire content is refluxed for 4 h. In an another set saturated solution of triphenylphosphine is prepared in ethanol and 20 ml of this saturated solution is refluxed with 1.5 g of modified R_6 resin for 4 h. After the completion of the reaction, the resin is washed and dried and is ready for examining the anion exchange capability. The reaction occurring during the above treatment can be written as:

(i) Reaction with trimethylamine (TMA):

$$\text{Ⓟ}-CH_2CHC_6H_4N(CH_2CH_2Cl)_2 \xrightarrow{TMA} \text{Ⓟ}-CH_2CHC_6H_4N(CH_2CH_2N^+(CH_3)_3Cl^-)_2$$

R_6 $\qquad\qquad$ R_7

Table 4.2: Experimental procedure on laboratory scale (1.5 g): Preparation of PMMA-EGDM resin

Step A: Gas phase nitration of PMMA-EGDM resin using NO_x

Direct gas phase nitration of PMMA-EGDM resin occurred efficiently in the presence of NO_2 with a small amount of NO and was carried out in a 2.5-L reaction bottle. This reaction vessel was equipped with an aluminium cap with a 1.2 mm opening at the top for injecting the gas, which was closed by a silicon rubber septum. By use of the method of Vogel and Cotton and Wilkinson, NO_2 with a minor amount of NO (termed NO_x) was generated in a 1.5-L two-neck round bottom flask by reacting sodium nitrite ($NaNO_2$, 10g, 0.14 g-mol) with sulfuric acid (H_2SO_4, sp. gr. 1.18, 25 ml) in the presence of ferrous sulfate ($FeSO_4$, 5 g, 0.072 g-mol). The reaction occurred at room temperature and the flask was equipped with a rubber septum for withdrawing NO_x with a 100 ml syringe.

The scheme of nitration was similar to that described in the literature and about 1.5 g of PMMA-EGDM resins were introduced into the reaction vessel placed in an oven maintained at the desired reaction temperature. A small needle was used to puncture the silicon rubber septum of the reactor so as to allow a thermal equilibrium with the oven without developing pressure in it. The gas inside the bottle expanded as a result of heating and escaped through the needle; after this, the needle was removed and the vessel was taken out and allowed to cool at room temperature. This created a slight vacuum inside the vessel on cooling so

that when NO_x was introduced into the bottle, at the reaction temperature, the total pressure remained at about 1 atm. After feeding the required amount of gas mixture, the vessel was again kept in the oven maintained at the reaction temperature. After completion of nitration the vessel was removed from the oven and allowed to cool to room temperature. If we represent PMMA-EGDM by resin 1 below, its nitration can be written as:

$$\text{(P)}-CH_2C(COOCH_3)CH_3 \xrightarrow{NO_X,\ 120^0C} \text{(P)}-CH_2C(COOCH_3)CH_2 - NO_2$$

Resin 1 Resin 2

Step B: Amination of PMMA-EGDM resins

To reduce the NO_2 functional group to amine groups on the surface of PMMA-EGDM resins, 1.5 g of resin 2 was heated with 50 ml hydrazine hydrate (85%) at 60 ^0C in a conical flask for 4 h. The resin's color changed from pale yellow to golden yellow after the amination reaction. Again, the chemical changes taking place on the resin can be represented by:

$$\text{(P)}-CH_2C(COOCH_3)CH_2 - NO_2 \xrightarrow{\text{Hydrazine hydrate } 50^0C} \text{(P)}-CH_2C(COOCH_3)CH_2 - NH_2$$

Resin 2 Resin 3

Table 4.3: Experimental results for different resins

Run	Experimental conditions	Anion Exchange Capacity (meq/g)
1	PS resin; Cast Iron drum; 23 sequential iterations of nitration on 1.5 kg resin	0.32
2	PS resin; when $FeSO_4$ and $NaNO_2$ are added to produce NO_x	0.38
3	PS resin; when $FeSO_4$ is added only once	0.39
4	PS resin; when $FeSO_4$ is not added at all	0.37
5	PS resin; NO_x used 400 ml/g of resin; amination using 40% HH at 60 ^{0}C for overnight	0.40
6	PS resin; NO_x used 500 ml/g of resin; amination using 40% HH at 60 ^{0}C for overnight	0.39
7	PS resin; NO_x used 600 ml/g of resin; amination using 40% HH at 60 ^{0}C for overnight	0.40
8	PS resin; NO_x used 300 ml/g of resin; 40% HH at 60 ^{0}C for 4 h	0.43
9	PS resin; NO_x used 300 ml/g of resin; 20% HH at 60 ^{0}C for 4 h	0.40
10	PS resin; NO_x used 300 ml/g of resin; 85% HH at 80 ^{0}C for 4 h	0.48
11	PMMA resin; when outside reactor temperature is 120 ^{0}C	0.26
12	PMMA resin; when temperature inside reactor is 120 ^{0}C	0.41
13	PMMA resin; vacuum created 1.2 cm Hg; After filling gas, pr. 7 cm Hg	0.85
14	PMMA resin; vacuum created 1.4 cm Hg; After filling gas, pr. 9.2 cm Hg	0.90
15	PMMA resin; vacuum created 2 cm Hg; After filling gas, pr. 15.8 cm Hg	0.39
16	PMMA resin; Al painted and foiled drum; when nitration is done using medical oxygen	0.37
17	PMMA resin; Al cladded drum; when nitration is using commercial oxygen	0.45

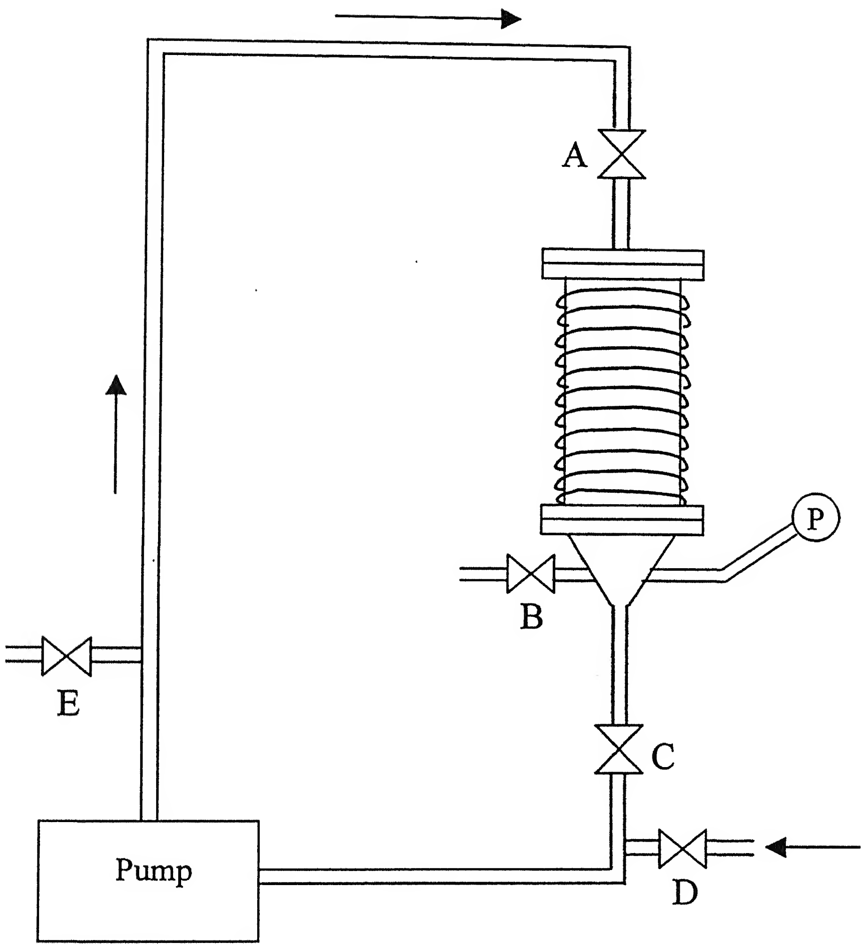

Figure 4.1: Experimental setup for the nitration of resin, provided by Jubilant Organosys Ltd.

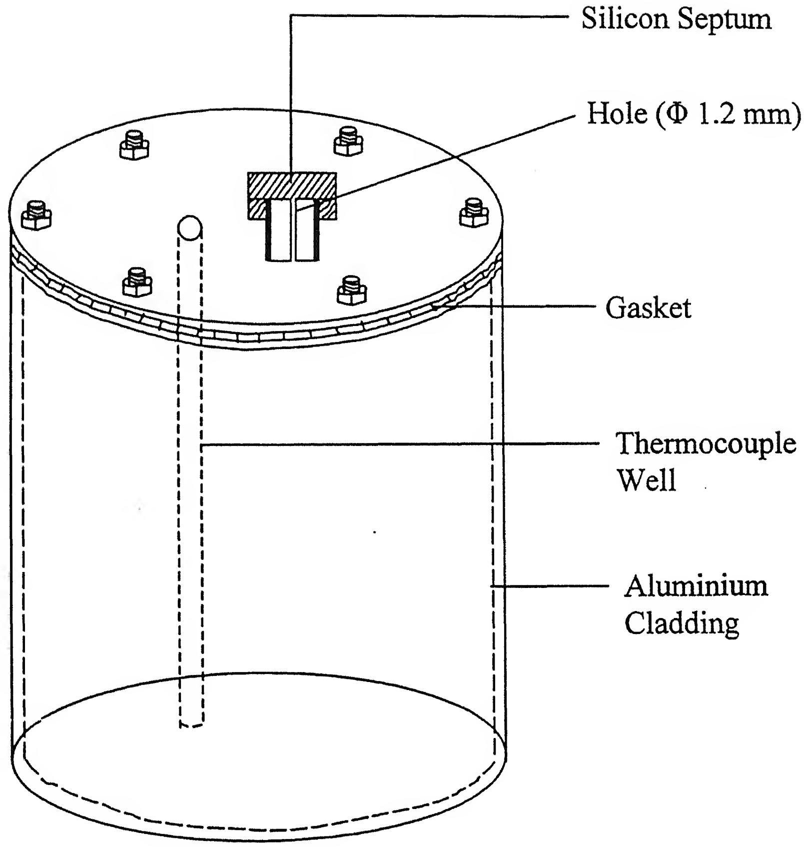

Figure 4.2: Schematic diagram of scaled up reactor

Chapter 5

CONCLUSIONS

An electrodialysis zeolite clay composite membrane has been successfully prepared by in-situ hydrothermal crystallization of Analcime C zeolite over the mesoporous clay support and modified by depositing $FeCl_2$ ions inside the pores. The resulting iron salt embedded membrane showed a significant improvement in current efficiency as compared to that of zeolite clay composite membrane in electrolysis of KCl solution. The effect of operating parameters (current density, circulation rate, salt and alkali concentration, and temperature) on the performance of the iron salt embedded membrane has been studied for KCl solution and these results have been compared with that of NaCl solution. The current efficiency for the membrane is found to decrease slightly for higher current densities, higher circulation rates and higher KOH concentrations, and to increase with increase in salt concentration. The membrane shows a significant improved performance in terms of current efficiency and energy consumption at higher temperatures which shows the thermal stability of membrane in contrast with polymeric membranes used for this purpose. It has also been found that for the operating variables (temperature and salt concentration of anolyte chamber) which on increasing, increase the current efficiency, KCl solution gives better results than NaCl solution while for the operating variables (current density and concentration of catholyte chamber) which on increasing, decrease the current efficiency, NaCl solution gives better results than KCl solution. Lastly, scale up of the reactor has been done for the nitration of PS-DVB and PMMA-EGDM resins.

REFERENCES

1. V.H. Thang, W. Koschuh, K.D. Kulbe, S. Novalin, Detailed investigation of an electrodialytic process during the separation of lactic acid from a complex mixture, J. Membr. Sci., 249 (2005) 173-182.

2. J.M. Ortiz, J.A. Sotoca, E. Exposito, F. Gallud, V. Garcia-Garcia, V. Montiel, A. Aldaz, Brackish water desalination by electrodialysis: batch recirculation operation modeling, J. Membr. Sci., 252 (2005) 65-75.

3. F. Quemeneur, J-P Schlumpf, L. Firdaous, M. Stitou, J-P Maleriat, P. Jaouen, Modification of ionic composition of natural salt-waters by electrodialysis, Desalination, 149 (2002) 411-416.

4. G.S. Luo, X.Y. Shan, X. Qi, Y.C. Lu, Two-phase electro-electrodialysis for recovery and concentration of citric acid, Sep. Purif. Technol., 38 (2004) 265-271.

5. L. Yu, T. Lin, Q. Guo, J. Hao, Relation between mass transfer and operation parameters in the electrodialysis recovery of acetic acid, Desalination, 154 (2003) 147-152.

6. V.M. Aponte, G. Colon, Sodium chloride removal from urine via a six-compartment ED cell for use in Advanced Life Support Systems (Part 1: Salt removal as a function of applied voltage and fluid velocity), Desalination, 140 (2001) 121-132.

7. V.M. Aponte, G. Colon, Sodium chloride removal from urine via a six-compartment ED cell for use in Advanced Life Support Systems (Part 2: Limiting current density behavior), Desalination 140 (2001) 133-144.

8. Marian Turek, Dual-purpose desalination-salt production electrodialysis, Desalination, 153 (2002) 377-381.

9. A. Tor, T. Buyukerkek, Y. Cengeloglu, M. Ersoz, Simultaneous recovery of Cr(III) and Cr(VI) from the aqueous phase with ion-exchange membranes, Desalination, 171 (2004) 233-241.

10. R.F.D. Costa, M.A.S. Rodrigues, J.Z. Ferreira, Transport of trivalent and hexavalent chromium through different ion-selective membranes in acidic aqueous media, Sep. Sci. Technol., 33(8) (1998) 1135-1143.

11. N. Tzanetakis, W.M. Taama, K. Scott, R.J.J. Jachuck, R.S. Slade, J. Varcoe, Comparative performance of ion exchange membranes for electrodialysis of nickel and cobalt, Sep. Purif. Technol., 30 (2003) 113-127.

12. Marian Turek, Electrodialytic desalination and concentration of coal-mine brine, Desalination, 162 (2004) 355-359.

13. H.K. Hansen, A. Rojo, L.M. Ottosen, Electrodialytic remediation of copper mine tailings, J. Hazard. Mater., B117 (2005) 179-183.

14. E. Korngold, L. Aronov, N. Belayev, K. Kock, Electrodialysis with brine solutions oversaturated with calcium sulfate, Desalination, 172 (2005) 63-75.

15. L. Bazinet, M. Araya-Farias, Effect of calcium and carbonate concentrations on cationic membrane fouling during electrodialysis, J. Colloid. Interf. Sci., 281 (2005) 188-196.

16. T. Mohammadi, A. Moheb, M. Sadrzadeh, A. Razmi, Separation of copper by electrodialysis using Taguchi experimental design, Desalination, 169 (2004) 21-31.

17. T. Mohammadi, A. Razmi, M. Sadrzadeh, Effect of operating parameters on Pb^{2+} seperation from wastewater using electrodialysis, Desalination, 167 (2004) 379-385.

18. L. Bazinet, Y. DeGrandpre, A. Porter, Electromigration of tobacco polyphenols, Sep. Purif. Technol., 41 (2005) 101-107.

19. H. Inoue, M. Kagoshima, M. Yamasaki, Y. Honda, Radioactive iodine waste treatment using electrodialysis with an anion exchange paper membrane, App. Radiat. Isotop., 61 (2004) 1189-1193.

20. F. Schaffner, P.-Y. Pontalier, V. Sanchez, F. Lutin, Comparison of diester waste treatment by conventional and bipolar electrodialysis, Desalination, 170 (2004) 113-121.

21. Q.Z. Du, M.J. Li, Q. Cheng, C.Y. Lu, The study on separation catechins from tea leaves and transforming gallate-catechins into nongallate-catechins, Res. Dev. Basic Agic. High Technol., 1 (1997) 40-47.

22. N. Tzanetakis , J. Varcoe , R.S. Slade , K. Scott; Salt splitting with radiation grafted PVDF anion-exchange membrane, Electrochem. Comm., 5 (2003) 115-119.

23. F.C. Nachod, Jack Schubert (eds), Ion Exchange Technology, Academic Press Inc., New York (1956) 121-126.

24. R.D. Noble, S.A. Stern (eds), Membrane Separations Technology: Principles and Applications, Elsevier, Amsterdam (1995) 213-263.

25. Y.-J. Choi, J.-M. Park, K.-H. Yeon, S.-H. Moon, Electrochemical characterization of poly(vinyl alcohol)/formyl methyl pyridinium (PVA-FP) anion-exchange membranes, J. Membr. Sci., 250 (2005) 295-304.

26. R. Wycisk, P.N. Pintauro, Sulfonated polyphosphazene ion-exchange membranes, J. Membr. Sci., 119 (1996) 155-160.

27. T. Xu, W. Yang, Fundamental studies on a novel series of bipolar membranes prepared from poly(2,6-dimethyl-1,4-phenylene oxide) (PPO) I. Effect of anion exchange layers on I-V curves of bipolar membranes, J. Membr. Sci., 238 (2004) 123-129.

28. Y. Oren, V. Freger, C. Linder, Highly conductive ordered heterogeneous ion-exchange membranes, J. Membr. Sci., 239 (2004) 17-26.

29. M.-S. Kang, Y.-J. Choi, I.-J. Choi, T.-H. Yoon, S.-H. Moon, Electrochemical characterization of sulfonated poly(arylene ether sulfone) (S-PES) cation-exchange membranes, J. Membr. Sci., 216 (2003) 39-53.

30. W. J. Chen, C. R. Martin, Gas-transport properties of sulfonated polystyrenes, J. Membr. Sci., 95 (1994) 51-61.

31. Q. Guo, P. N. Pinturo, Sulfonated and cross-linked polyphosphazene based proton exchange membranes, J. Membr. Sci., 154 (1999) 175-181.

32. M. M. Nasef, H. Saidi, Preparation of crosslinked cation exchange membranes by radiation grafting of styrene/divinylbenzene mixtures onto PFA films, J. Membr. Sci., 216 (2003) 27-38.

33. N. Tzanetakis, W. M. Taama, K. Scott, J. Varcoe, R. S. slade, Salt splitting with radiation grafted PVDF membranes, Desalination,151 (2002) 275-282.

34. L. M. Cormier, F. Ma, S. T. Bah, S. Guetre, M. Meunier, Sodium salt-splitting performance of a novel ceramic-polymer composite cation-selective membrane, J. Electrochem. Soc., 149(1) (2002) D21-D26.

35. R. Izquierdo, E. Quenneville, D. Trigylidas, F. Girard, M. Meunier, D. Ivanov, M. Paleologou, A. Yelon, Pulsed Laser Deposition of NASICON thin films for the fabrication of ion selective membranes, J. Electrochem. Soc., 144(12) (1997) L323-L325.

36. K. C. Popat, E. E. L. Swan, V. Mukhatyar, K.-I. Chatvanichkul, G. K. Mor, C. A. Grimes, T. A. Desai, Influence of nanoporous alumina membranes on long-term osteoblast response, Biomaterials, 26 (2005) 4516-4522.

37. Y. Piao, H. Lim, J. Y. Chang, W.-Y. Lee, H. Kim, Nanostructured materials prepared by use of ordered porous alumina membranes, Electrochim. Acta, 50 (2005) 2997-3013.

38. Q. Wang, G. Wang, B. Xu, J. Jie, X. Han, G. Li, Q. Li, J.G. Hou, Non-aqueous cathodic electrodeposition of large-scale uniform ZnO nanowire arrays embedded in anodic alumina membrane, Mat. Lett., 59 (2005) 1378-1382.

39. C. Falamaki, M. Naimi, A. Aghaie, Dual behavior of $CaCO_3$ as a porosifier and sintering aid in the manufacture of alumina membrane/catalyst supports, J. Europ. Ceramic Soc., 24 (2004) 3195-3201.

40. A. A. Babaluo, M. Kokabi, M. Manteghian, R. Sarraf-Mamoory, A modified model for alumina membranes formed by gel-casting followed by dip-coating, J. Europ. Ceramic Soc., 24 (2004) 3779-3787.

41. K. Kusakabe, S. Fumio, T. Eda, M. Oda, K.-I. Sotowa, Hydrogen production in zirconia membrane reactors for use in PEM fuel cells, Int. J. Hydrog. Energy, 30 (2005) 989-994.

42. V.M. Linkov, V. N. Belyakov, Novel ceramic membranes for electrodialysis, Sep. Purif. Technol., 25 (2001) 57-63.

43. D. E. Kurath, K. P. Brooks, G. W. Hollenberg, D. P. Sutija, T. Landro, S. Balagopal, Caustic recycle from high-salt nuclearwastes using a Ceramic-membrane salt-splitting process, Sep. Purif. Technol., 11 (1997) 185-198.

44. F. Girard, R. Quenneville, S. T. Bah, M. Paleologou, M. Meunier, D. Ivanov, A. Yelon, Evaluation of a ceramic-polymer composite cation-selective membrane for sodium salt splitting, J. Electrochem. Soc., 146(8) (1999) 2919-2924.

45. C. S. Cundy, P. A. Cox, The hydrothermal synthesis of zeolites: History and development from the earliest days to the present time, Chem. Rev., 103 (2003) 663-701.

46. M.-D. Jia, K.-V. Peinemann, R.-D. Behling, Ceramic zeolite composite membranes, J. Membr. Sci., 82 (1993) 15-26.

47. M.-D. Jia, B. Chen, R. D. Noble, J. L. Falconer, Ceramic-zeolite composite membranes and their application for separation of vapor/gas mixtures, J. Membr. Sci., 90 (1994) 1-10.

48. J. M. Van de Graaf, F. Kapteijn, J. A. Moulijn, Modeling permeation of binary mixtures through zeolite membranes, AIChE J., 45(3) (1999) 497-511.

49. Y. H. Ma, Y. Zhou, R. Poladi, E. Engwall, The synthesis and characterization of zeolite A membranes, Sep. Purif. Technol., 25 (2001) 235-240.

50. A. Potdar, A. Shukla, A. Kumar, Effect of gas phase modification of analcime zeolite composite membrane on separation of surfactant by ultrafiltration, J. Membr. Sci., 210 (2002) 209-225.

51. Anupam Shukla, Preparation, Modification and Application of zeolite-clay composite membrane, PhD Thesis, IIT Kanpur, August (2003).

52. D. P. Siantar, W. S. Millman, J. J. Fripiat, Structure defects and cation exchange capacity in dealuminated Y zeolite, Zeolites, 15 (1995) 556-560.

53. X. Xu, W. Yang, J. Liu, L. Lin, Synthesis of NaA zeolite membranes from clear solution, Micropor. Misopor. Mat., 43 (2001) 299-311.

54. B.J. Schoeman, J. Sterte, J. E. Otterstedt, Synthesis and size tailoring of colloidal zeolite particles, Chem. Commun., 12 (1993) 994-995.

55. Y.H. Ma, S. Xiang, Formation and characterization of zeolite membranes from sols, Abstract, Third Intl. Conference on Inorganic Membranes, Worcester, MA, July(1994) 10-14.

56. G. Xomeritakis, A. Gouzinis, S. Nair, T. Okubo, M. He, R. M. Overney, M. Tsapatsis, Growth, microstructure and permeation properties of supported zeolite (MFI) films and membranes prepared by secondary growth, Chem. Eng. Sci., 54 (1999) 3521-3531.

57. Harry Robson (ed), Verified syntheses of zeolitic materials, Second revised edition, Karl Petter Lillerud, XRD patterns, Elsevier, Amsterdam (2001) 107.

58. S.D. Han, J.K. Kim, K.C. Singh, R.S. Chaudhary, Electrochemical generation of ozone using solid polymer electrolyte-State of the art, Ind. J. Chem., 43A (2004) 1599-1614.

59. J. Joo, T. Hyeon, J. Hyeon-Lee, Fabrication of novel mesoporous dimethylsiloxane-incorporated silicas, Chem. Commun., 21 (2000) 1487-1488.

60. P. C. Jain, Monika Jain, Engineering Chemistry, 11^{th} edition, (1998) 32-37.

61. R. G. Shaikh, Study of modification of flyash zeolite using NO_x, M. Tech. Thesis, IIT Kanpur, (2000) 10-15.

62. E. Jakobs, W.J. Koros, Ceramic membrane characterization via the bubble point technique, J. Membr. Sci., 124 (1997) 149-159.

63. T. Aritomi, Th. van den B., H. Strathmann, Current-voltage curve of a bipolar membrane at high current density, Desalination, 104 (1996) 13-18.

64. F. G. Wilhelm, N. F. A. van der Vegt, M. Wessling, H. Strathmann, Chronopotentiometry for the advanced current-voltage characterization of bipolar membranes, J. Electroanal. Chem., 502 (2001) 152-166.

65. Manoj Kumar, Electrolysis of sodium chloride solution using iron salt embedded ultrafiltration zeolite clay composite membrane, M. Tech. Thesis, IIT Kanpur, July (2004).

66. J. S. Reed, Introduction to the principles of ceramic processing, John Wiley & Sons, New York, 1989.

67. Powder Diffraction files, International centre for Diffraction Data, Pennsylvania, USA.

68. M.-S. Kang, Y.-J. Choi, H.-J. Lee, S.-H. Moon, Effects of inorganic substances on water splitting in ion-exchange membranes: I. Electrochemical characteristics of ion-exchange membranes coated with iron hydroxide/oxide and silica sol, J. Colloid. Interf. Sci., 273 (2004) 523-532.

69. O. P. Agarwal, IIT Chemistry, Jaiprakash Nath Publications, Meerut (1993) 555.

70. N. Tzanetakis, W. M. Taama, K. Scott, Salt splitting in a three-compartment membrane electrolysis cell, Filtration & Separation, April (2002) 31-38.

71. D. T. Hobbs, J. L. Steimke, D. E. Kurath, S. Balagopal, T. Landro, D. P. Sutija, J. D. Genders, D. Chai, Recovery of Sodium Hydroxide from Alkaline Waste Solutions, U. S. Department of energy, WSRC-MS-98-00532.

72. Shishir Sinha, Study of molecularly different and efficient macroporous, strong base anion exchange resin by gas phase modification using NO_x, PhD Thesis, IIT Kanpur, July (1999).